DOI: 10.1002/cmdc.201100166

Toward the Discovery of Novel Anti-HIV Drugs. Second-Generation Inhibitors of the Cellular ATPase DDX3 with Improved Anti-HIV Activity: Synthesis, Structure–Activity Relationship Analysis, Cytotoxicity Studies, and Target Validation

Giovanni Maga,[b] Federico Falchi,[a] Marco Radi,[a] Lorenzo Botta,[a] Gianni Casaluce,[a] Martina Bernardini,[a] Hamid Irannejad,[a] Fabrizio Manetti,[a] Anna Garbelli,[b] Alberta Samuele,[b] Samantha Zanoli,[b] José A. Esté,[c] Emmanuel Gonzalez,[c] Elisa Zucca,[b] Stefania Paolucci,[d] Fausto Baldanti,[d] Jan De Rijck,[e] Zeger Debyser,[e] and Maurizio Botta*[a, f]

A hit optimization protocol applied to the first nonnucleoside inhibitor of the ATPase activity of human DEAD-box RNA helicase DDX3 led to the design and synthesis of second-generation rhodanine derivatives with better inhibitory activity toward cellular DDX3 and HIV-1 replication. Additional DDX3 inhibitors were identified among triazine compounds. Biological data were rationalized in terms of structure–activity relationships and docking simulations. Antiviral activity and cytotoxicity of selected DDX3 inhibitors are reported and discussed. A thorough analysis confirmed human DDX3 as a valid anti-HIV target. The compounds described herein represent a significant advance in the pursuit of novel drugs that target HIV-1 host cofactors.

Introduction

Viruses are obligate intracellular parasites that hijack the metabolic machinery of their host cells in order to replicate and propagate the infection. Functional genomic screenings have recently identified about 300 human proteins important for the replicative cycle of human immunodeficiency virus type 1 (HIV-1).[1,2] Such previously unrecognized complexity of host–pathogen relationships, coupled to the seemingly unavoidable problem of drug resistance due to the high mutation rate of HIV-1, has renewed the long-standing interest toward cellular proteins as novel targets for the treatment of HIV-1 infection.[3,4] The main argument in favor of targeting a host factor instead of a viral protein is the predicted low drug resistance level. On the other hand, interfering with a cellular pathway might lead to serious complications, including crucial cell function loss or oncogenic drift. Thus, it is of paramount importance to identify host cell factors that, while absolutely essential for the virus, are dispensable for the host cell metabolism. One protein that has recently attracted much attention is the human DEAD-box RNA helicase DDX3.[5–7] It has been reported that four different viruses, hepatitis C virus (HCV), hepatitis B virus (HBV), HIV, and poxviruses encode proteins that can interact with DDX3 to modulate its functions. For this reason, DDX3 seems a prime target for viral manipulation. In addition, while DDX3 has been implicated in many aspects of RNA metabolism, such as mRNA export, transcriptional regulation and translation, several studies have shown that DDX3 knockdown did not result in cellular toxicity, at least in cell culture models.[8–12]

In the case of HIV-1, it has been shown that knockdown of DDX3 suppressed viral replication due to a block of the Rev-dependent export of unspliced or partially spliced viral

[a] Dr. F. Falchi, Dr. M. Radi, Dr. L. Botta, Dr. G. Casaluce, Dr. M. Bernardini, Dr. H. Irannejad, Dr. F. Manetti, Prof. M. Botta
Dipartimento Farmaco Chimico Tecnologico
University of Siena, Via Alcide de Gasperi 2, 53100 Siena (Italy)
Fax: (+39) 0577-234-306
E-mail: botta.maurizio@gmail.com

[b] Dr. G. Maga, Dr. A. Garbelli, Dr. A. Samuele, Dr. S. Zanoli, Dr. E. Zucca
Istituto di Genetica Molecolare, IGM-CNR
Via Abbiategrasso 207, 27100 Pavia (Italy)

[c] Prof. J. A. Esté, Dr. E. Gonzalez
Retrovirology Laboratory IrsiCaixa
Hospital Universitari Germans Trias i Pujol
Universitat Autónoma de Barcelona, 08916 Barcelona (Spain)

[d] Dr. S. Paolucci, Dr. F. Baldanti
Molecular Virology Unit, Foundation IRCCS Policlinico S. Matteo
piazzale Golgi, 27100 Pavia (Italy)

[e] Dr. J. De Rijck, Prof. Z. Debyser
Molecular Medicine, Katholieke Universiteit Leuven and IRC KULAK
Kapucijnenvoer 33, 3000 Leuven, Flanders (Belgium)

[f] Prof. M. Botta
Sbarro Institute for Cancer Research and Molecular Medicine
Temple University, BioLife Science Building
Suite 333, 1900 N. 12th St., Philadelphia, PA 19122 (USA)

Supporting information for this article is available on the WWW under http://dx.doi.org/10.1002/cmdc.201100166.

mRNAs.[10] Based on these considerations, our group has undertaken a rational drug design approach aimed at finding small molecules able to suppress DDX3 activity. Because no inhibitors of any DEAD-box helicase are known, a structure-based pharmacophore modeling and molecular docking protocol applied to the X-ray crystallographic structure of the human helicase DDX3 in complex with AMP[13] was set to search, within the Asinex Gold collection,[14a] small-molecule inhibitors of the ATPase activity of DDX3. As a result of such simulations, hit compounds belonging to the class of rhodanine derivatives were found. One of these compounds (**4a**) showed low micromolar potency of inhibition against the DDX3 ATPase activity and was able to confer protection to human cells when challenged with HIV-1, albeit at substantially higher doses.[11] This was the first sucessful identification of a nonnucleoside analogue able to interfere with HIV-1 replication by targeting a cellular enzyme. Almost simultaneously, another study identified ring-expanded nucleoside inhibitors of the DDX3 helicase activity as potential anti-HIV-1 agents.[15] The interaction pattern between the ATPase pocket and the rhodanine-based hit compound **4a** (Figure 1 A) showed its 2-OH substituent at R^1 embedded within a polar pocket (thereafter referred to as the right pocket) and involved either as a hydrogen bond acceptor or donor group in interactions with the backbone NH group of Gly 229, Lys 230, and Ser 228, and with the terminal carbonyl oxygen of Gln 225, respectively. An additional anchor point was represented by the rhodanine carbonyl oxygen that interacted with the terminal NH_2 group of Gln 207. Hydrophobic interactions between the terminal bromophenyl moiety and a region (thereafter referred to as the left pocket) mainly defined by the alkyl chain of Arg 202 and Glu 523, as well as possible π–π contacts between the rhodanine heterocycle and the Tyr 200 phenyl ring further stabilized the complexes. Electrostatic interactions between the bromo substituent and the terminal guanidino group of Arg 202 were also found.

Here we present the results of a hit optimization process leading to the design, synthesis, and biological characterization of second-generation DDX3 inhibitors endowed with higher potencies against both the target cellular enzyme and HIV-1 replication. In addition, we have carefully re-evaluated the effects of DDX3 knockdown in human cells, providing further support for DDX3 as a promising target for anti-HIV chemotherapy.

Results and Discussion

Chemistry

Based on the proposed binding mode of the hit **4a**, a series of analogues were synthesized following the classical synthetic approach[16] reported in Scheme 1. This first set of derivatives is

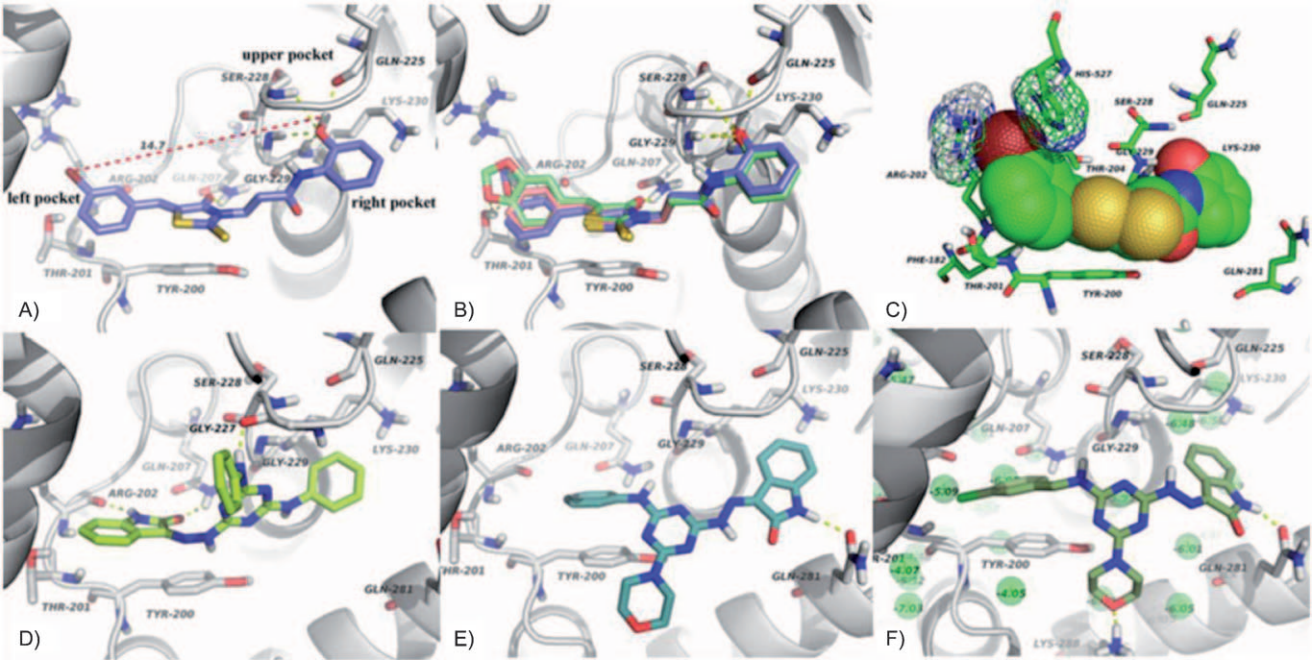

Figure 1. Representation of the binding mode of rhodanine and triazine derivatives within the DDX3 ATP binding site. Hydrogen bond interactions are represented by yellow dashed lines. Regions of best interactions with chloride probes are green spheres. A) Best pose for **4a**. The distance between the 2-OH and the 3-Br is represented as a red dashed line. The right, upper, and left sites of the binding site are labeled. B) Oxygen atoms of **4f** (green) and **4e** (blue) are important anchor points to interact with the left site. Also the fluorine of **4b** (pink) lyes in the same region of space where electrostatic interactions are allowed with the guanidino group of Arg 202 and where one important minimum energy point for the fluorine probe (-3.88 kcal mol^{-1}, see Figure 2 C) was found by GRID. C) Representation of the interaction pattern between **4a** (CPK notation) and the left pocket. The bromo substituent is embedded between the Arg 202 and His 727 side chain, suggesting profitable electrostatic interactions. Contacts with the polymethylenic portion of the Arg 202 side chain are also shown. D) Our first triazine derivative (**15a**) identified by high-throughput docking simulations. E) Inactive compound **15b** only maintains the interaction with Gln 281 and a possible stacking with Tyr 200. F) The chloride of **15f** restores a significant activity, accounted for the interaction with a region of best interaction found by GRID for the chloride probe. Higher-resolution images are available in the Supporting Information.

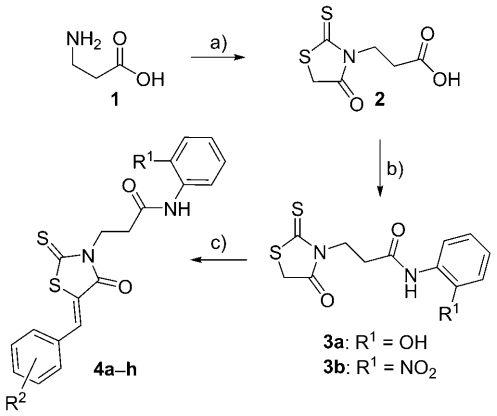

Scheme 1. Synthesis of rhodanine derivatives **4a–h**. *Reagents and conditions*: a) CS_2, $BrCH_2COOH$, 22% aq. KOH, RT, 6 h; b) pivaloyl chloride, DIPEA, 2-aminophenol, 1,2-dichloroethane, RT, 18 h (for **3a**), $SOCl_2$, 2-nitroaniline, CH_2Cl_2, RT, 2 h (for **3b**); c) R^2PhCHO, EtOH, Et_3N, 1 h, reflux (Method A), R^2PhCHO, MW, 130 °C, 5 min (3 cycles) (Method B).

characterized by a few focused modifications on the two aromatic rings of the hit. The synthesis of the rhodanine derivatives **4a–h** started from commercially available β-alanine **1** that was allowed to react with carbon disulfide and α-bromoacetic acid in basic medium to give the N-substituted rhodanine scaffold **2**. This intermediate was then coupled with two substituted anilines to give compounds **3a,b** which were finally treated with various benzaldehydes, under classical or microwave-assisted Knoevenagel conditions, to give the desired final compounds **4a–h**.

A second set of analogues of **4a**, characterized by an inverted amide moiety and by the replacement of the rhodanine with a different scaffold, was also synthesized. Considering that a preliminary enzymatic screening[11] identified **4a** and **4b** as the most interesting derivatives, the synthesis of their corresponding inverted amide analogues **7a,b** was attempted (Scheme 2). After some initial failures with the classical procedure reported above, a fast and efficient one-pot, two-step protocol was developed, combining the "Holmberg method" and the Knoevenagel condensation under microwave-assisted conditions.[17] As a result, the desired inverted amide derivatives **7a,b** were obtained in high yield and purity by reacting bis(carboxymethyl)trithiocarbonate **5** with the amine **6**, synthesized following a reported procedure.[18]

Looking for a different scaffold to replace the rhodanine moiety of **4a**, we selected the succinimide moiety as a valuable alternative. The synthesis of the desired derivative **11** started from commercially available 3-bromobenzaldehyde **8** which was transformed into the anhydride **9** passing through the (*E*)-benzylidenesuccinic acid intermediate (Scheme 3).[19] Treatment

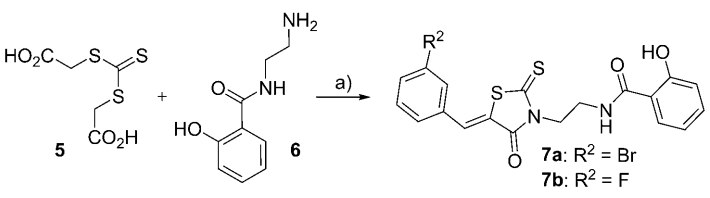

Scheme 2. Synthesis rhodanine derivatives **7a,b**. *Reagents and conditions*: a) 1. DME, Et_3N, 90 °C, MW, 10 min, 2. R^2PhCHO, 110 °C, MW, 5 min.

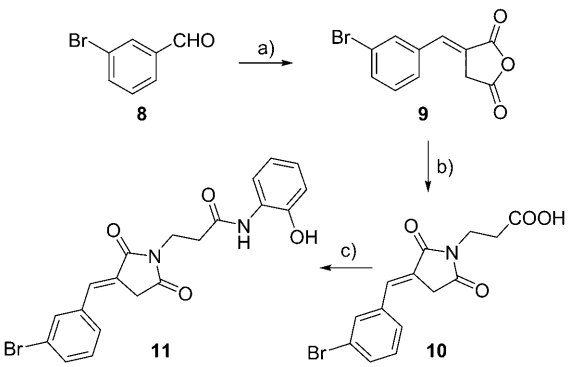

Scheme 3. Synthesis of succinimide derivative **11**. *Reagents and conditions*: a) 1. Diethyl succinate, *t*BuOH/*t*BuOK, reflux, 2 h, 2. 10% aq. NaOH, reflux, 4 h, 3. Ac_2O, THF, RT, 5 h; b) β-alanine, DMF, MW, 150 °C, 10 min; c) pivaloyl chloride, DIPEA, 2-aminophenol, 1,2-dichloroethane, RT, 18 h.

of the anhydride **9** with β-alanine under microwave-assisted conditions, followed by a coupling reaction with 2-aminophenol, afforded the desired final compound **11**.

A triazine-based series of derivatives was then synthesized after the identification of the hit compounds **15a** and **16h** (see Table 2 below) by a high-throughput docking approach (HTD; see the next section for details). These hits were characterized by two important pharmacophoric groups (namely, the indolyl-2-one and the 2-hydroxyphenyl moieties) connected via a hydrazone spacer to the central triazine scaffold. In addition, considering the positive contribution of the morpholino group of **16h** to the solubility of such compounds, we decided to synthesize two sets of triazine derivatives characterized by the presence of both the morpholine substituent and one of the two above mentioned pharmacophoric moieties. The synthetic approach to obtain such 2,4,6-trisubstituted-1,3,5-triazines was dependent on the type of amine to be introduced in the last available position of the triazine core. The benzylamino derivatives **15e–g** and **16i,j,o,p** were obtained by consecutive nucleophilic substitution of commercially available cyanuric chloride **12** (Scheme 4).

The first chlorine of **12** was displaced with the moderately nucleophilic benzylamines at −30 °C for 3 h to give the monosubstituted triazines **13a–c**. Subsequent treatment with a more nucleophilic amine provided the disubstituted triazines **14a–d**. The remaining chlorine of disubstituted triazines was replaced by treatment with excess hydrazine at reflux to afford the corresponding 2,4,6-trisubstituted triazine intermediates, which were finally allowed to react with the two selected pharmacophoric moieties (salicyl aldehyde or isatin) to give the final compounds **15e–g** and **16i,j,o,p**, respectively.

The above reported synthetic approach was then applied to the synthesis of the aniline derivatives **16m** and **20b,c** (Scheme 5). Unfortunately, reacting

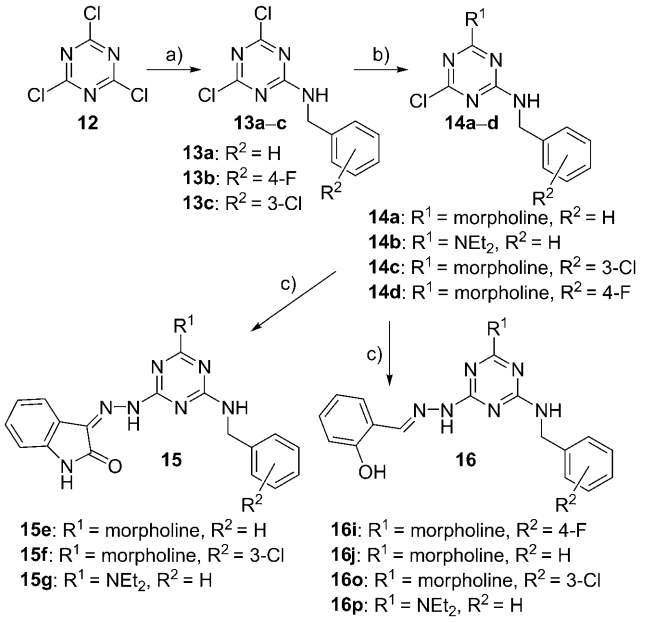

Scheme 4. Synthesis of triazine derivatives **15e–g**, **16i–p**. *Reagents and conditions*: a) DME, −30 °C, R^2BnNH_2, 3 h; b) CH_2Cl_2, R^1NH, RT, 12 h; c) 1. CH_2Cl_2, $NH_2NH_2{\cdot}H_2O$, reflux, 12 h, 2. toluene, isatin (for **15**) or salicylaldehyde (for **16**), 3 h, reflux, Dean–Stark.

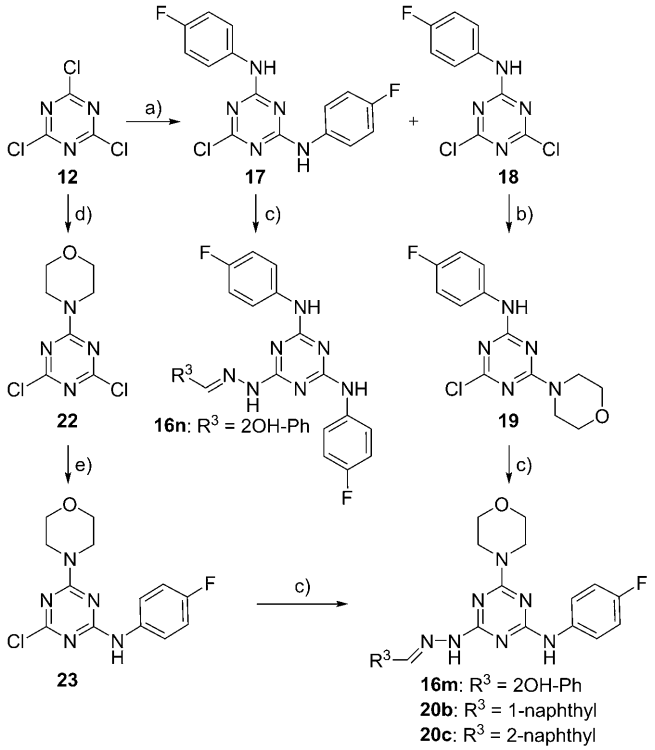

Scheme 5. Synthesis of triazine derivatives **16m,n**, **20b,c**. *Reagents and conditions*: a) DME, −30 °C, 4-fluoroaniline, 3 h; b) CH_2Cl_2, morpholine, RT, 12 h; c) 1. CH_2Cl_2, $NH_2NH_2{\cdot}H_2O$, reflux, 12 h, 2. toluene, R^3CHO, 3 h, reflux, Dean–Stark; d) DME, morpholine, 3 h, −30 °C; e) CH_2Cl_2, 4-fluoroaniline, 12 h, reflux.

cyanuric chloride with 4-fluoroaniline at −30 °C always resulted in a mixture of the disubstituted and monosubstituted derivatives **17** and **18**. Nevertheless, following the synthetic steps previously described, the intermediates **17** and **18** were converted into the final compounds **16n** and **20b**. A different sequence of nucleophilic substitutions on cyanuric chloride was then followed in order to cleanly obtain the aniline derivatives **16m** and **20b,c**. In brief, an initial treatment of **12** with morpholine followed by a nucleophilic substitution with 4-fluoroaniline and then with hydrazine gave the trisubstituted hydrazine intermediates, which were finally condensed with a small set of aromatic aldehydes to give the final compounds **16m** and **20b,c** as pure products.

Finally, we decided to synthesize analogues of the 2,4,6-trisubstituted-1,3,5-triazines having the triazine scaffold replaced by a pyrimidine nucleus. Based on our expertise on the functionalization of the pyrimidine scaffold[20] and taking into account the pharmacophoric requirements for the interaction with the ATP binding site of DDX3, **30** was considered as an interesting candidate to be synthesized (Scheme 6). Starting from the tosyl derivative **24**,[20b] available as intermediate in our lab, a microwave-assisted nucleophilic substitution with 4-fluoroaniline afforded the C4-substituted derivative **25**. The latter compound was oxidized to sulfone **26**, protected as the TBDPS ether **27**, and treated with hydrazine under microwave irradiation to give the intermediate **28**. Compound **28** was then condensed with salicylaldehyde to give **29** which was finally deprotected with triethylamine trihydrofluoride to give the final compound **30**.

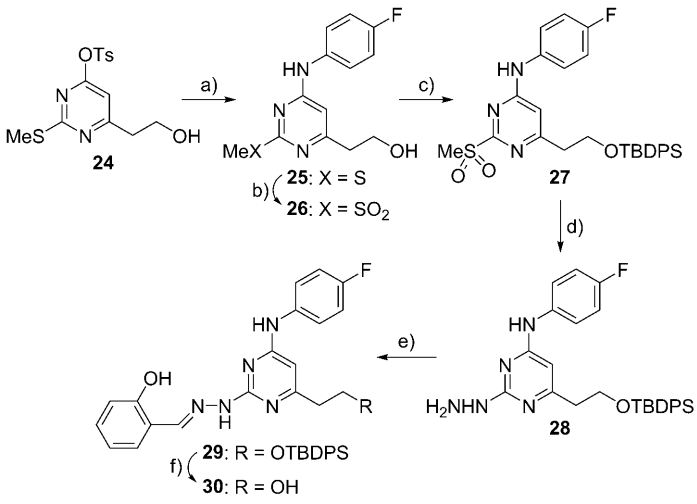

Scheme 6. Synthesis of pyrimidine derivative **30**. *Reagents and conditions*: a) 4-fluoroaniline, DME, MW, 150 °C, 5 min; b) Oxone, H_2O/MeOH/THF; c) TBDPSCl, DMF, imidazole, MW, 100 °C, 5 min; d) $NH_2NH_2{\cdot}H_2O$, DME, MW, 120 °C, 5 min; e) salicylaldehyde, toluene, molecular sieves, reflux, overnight; f) $Et_3N{\cdot}3HF$, THF, RT, overnight.

Structure–activity relationships for the second-generation DDX3 inhibitors

In addition to the compounds synthesized as described in the previous section, SciFinder Scholar[21] was used to search commercially available analogues of **4a**. As a result, many rhodanine derivatives were identified and obtained from commercial

sources (in particular, from Asinex and ChemBridge Corporation)[14b] to have a more complete set of derivatives for SAR considerations (Table 1). Results from docking calculations on rhodanine analogues suggested that the major interactions involved both molecular edges that are located within the left and right pocket of the ATP binding site on DDX3 (Figure 1 A).

Moreover, the distance of ~15 Å between the bromine and the hydroxy substituents of **4a**, taken as a representative compound, seemed to be optimal for the interaction with the protein. An ethyl spacer ($n=2$ as in **4a**) had the optimal length to allow the edges of ligands to make profitable hydrophobic and hydrogen bond contacts with the amino acids of the ATP binding site. In fact, variation of this length was detrimental for the activity (**4a** vs. **4x** as well as **4u** vs. **4y** and **4z**, Table 1). These results suggested that R^1 should be located at the right distance of ~15 Å from electron-rich substituents at R^2. At the right edge of the inhibitor structure, for certain substituents at R^2, replacement of the 2-OH group at R^1 with a 2-NO_2 (**4g** and **4h**) and 2-COOH (**4s** and **4t**) groups gave compounds of similar or slightly improved activity (**4g** vs. **4a** and **4s** vs. **4f**, Table 1). The configuration of the double bond at C5 also had a significant impact on the affinity toward the enzyme as it can be appreciated from the low activity of the *Z*-derivative **4r** bearing a 2-COOH at R^1. On the contrary, the methoxy derivative **4q** was inactive at the test dose (500 μM) probably because the terminal methyl group caused a steric clash with the protein, avoiding the oxygen atom of the methoxy group to behave as a hydrogen bond acceptor, as shown by docking simulations. In addition, the position of the OH group on the phenyl ring had a significant influence on the activity. In fact, while the 2-OH derivative **4a** showed a good affinity toward the enzyme, the 3- and 4-OH analogues (**4u**,**w**) showed a dramatic decrease in affinity. Moreover, replacement of the 2-OH group of **4l** with a chlorine led to **4m** with a significantly decreased activity (~40-fold).

Table 1. Structures and biological data for the new rhodanine derivatives.

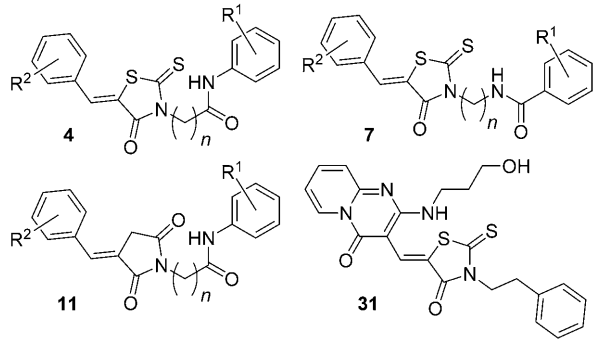

Compd	*n*	R^1	R^2	K_i[a] [μM]
4a[b]	2	2-OH	3-Br	5.4
4b	2	2-OH	3-F	0.3
4c	2	2-OH	3,5-diF	0.5
4d	2	2-OH	3-Me	97
4e	2	2-OH	3-OMe	10
4f	2	2-OH	3-(O-CH_2-O)-4	1.0
4g	2	2-NO_2	3-Br	8.7
4h	2	2-NO_2	3-F	7.6
4i[c]	2	2-OH	H	NA
4j[c]	2	2-OH	2-Cl	NA
4k[b]	2	3-OH	H	NA
4l[b]	2	2-OH	3,4,5-triOMe	0.1
4m[b]	2	2-Cl	3,4,5-triOMe	3.9
4n[c]	2	2-OH	4-Me	NA
4o[c]	2	2-OH, 3-Cl	4-Me	NA
4p[b]	2	2-OH, 5-Cl	4-OMe	11
4q[b]	2	2-OMe	3-Br	NA
4r[c,d]	2	2-COOH	3-Br	200
4s[b]	2	2-COOH	3-(O-CH_2-O)-4	0.4
4t[b]	2	2-COOH	4-OMe	2.0
4u[b]	2	3-OH	3-Br	90
4v[b]	2	3-OH	2-OMe	200
4w[b]	2	4-OH	3-Br	300
4x[b]	3	2-OH	3-Br	500
4y[c]	1	3-OH	3-Br	NA
4z[b]	3	3-OH	3-Br	150
7a	2	2-OH	3-Br	4.2
7b	2	2-OH	3-F	4.3
11	2	2-OH	3-Br	28
31	–	–	–	0.2

[a] Apparent equilibrium dissociation constant for the inhibitor to the target enzyme DDX3. [b] Purchased from Asinex. [c] Purchased from ChemBridge. [d] The double bond at C5 has an *E* configuration.

At the left edge, the 3-substituent at R^2 is able to contact either the guanidino moiety of Arg 202 or the hydrophobic polymethylenic chain of the same residue, as well as the imidazole ring of His 527 (Figure 1 C). On this basis, the good activity of the 3-F derivatives **4b** and **4c** relative to **4a** is not surprising if one takes into account the better electrostatic interactions. Moreover, similar interactions are possible between the guanidino group of Arg 202 and the oxygen atoms of methoxy (**4e**, **4l**, **4m**, **4p**, and **4t** that showed activities similar to that of **4a**) and dioxole derivatives (**4f** and **4s**). In fact, either such oxygen atoms or the fluorine substituent of **4b** and **4c** are accommodated within the same pocket, as also shown in Figure 1 B. A minimum energy point for the fluorine probe was found by GRID software[22] (Figure 2 C) in correspondence of this pocket. Docking simulations accounted for the importance of methoxy substituents accommodated within the left pocket of the binding site, the oxygen atom of the methoxy groups being located within the same region occupied by the fluoro group of **4b**, where electron-rich substituents should lie. Accordingly, the unsubstituted derivatives **4i** and **4k** lacked the contacts with the side chain of Arg 202, thus explaining its inactivity. The methyl group of **4d** restored some activity (97 μM) because of the hydrophobic contacts with the polymethylene chain of Arg 202, while changing the substitution pattern of the methyl group from position 3 to 4 resulted in inactive compounds such as **4n** and **4o**. This detrimental effect was probably due to the fact that the 4-methyl substituent was pointing toward the solvated interface between DDX3 monomers and, in several poses, showed steric clashes with the polymethylenic chain of Arg 202.

In a similar way, the 2-Cl substituent of **4j** showed steric clashes with the backbone of Arg 202 or, upon rotation of the phenyl ring at R^2, with the backbone of Tyr 200, resulting in an inactive compound. SAR considerations are unable to account for the little effect on potency observed upon replacing a 3-Br

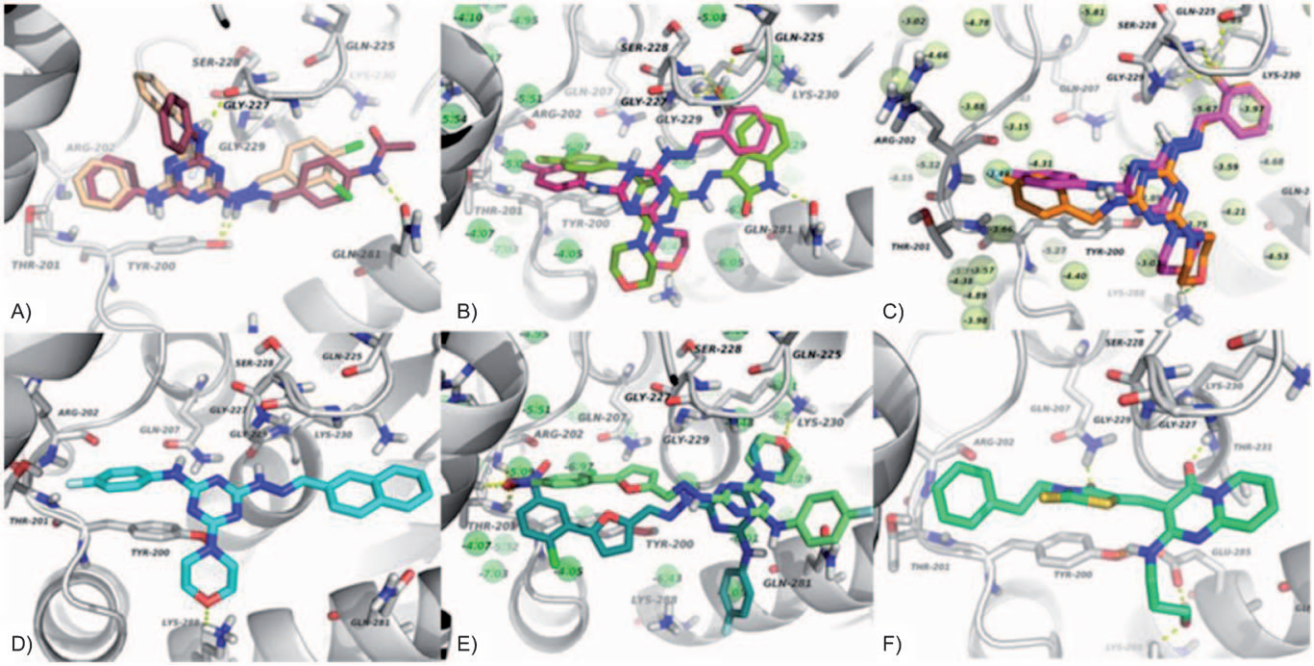

Figure 2. Representation of the binding mode of additional triazine derivatives within the DDX3 ATP binding site. Hydrogen bond interactions are represented by yellow dashed lines. Regions of best interactions with chloride and fluoride probes are green spheres, while those with hydrophobic probes (mimicking a methyl group) are grey spheres. A) The acetamido group of **16e** (brown) is very important for activity. Lack of hydrogen bond contacts within the right pocked leads to a decrease in activity of at least one order of magnitude (**16b**, pale brown). B) A very similar orientation and interaction pattern accounts for the similar activity of the benzylidene derivative **16h** (red) and the indolinone analogue **15d** (green). Their 3-Cl substituent is located within a minimum energy point (-6.97 kcal mol^{-1}) found by GRID for the chlorine probe. C) The difference between the benzylamino chain of **16i** (orange) and the anilino chain of **16m** (magenta) is not important for activity. Their 4-F substituent is located in a region of space where a minimum for the fluoride probe (-3.49 kcal mol^{-1}) was found. D) The 2-naphthyl moiety of **20c** is located within a large hydrophobic region in part corresponding to the right pocket. E) Changing the substitution pattern of the nitro group from position 4 (**21a**, light green) to 3 (**21b**, green) induces a conformational rearrangement of the terminal phenyl ring with a consequent decrease in activity. F) The phenylethyl rhodanine moiety of **31** is reminiscent of rhodanine derivatives **4**, while the hydroxypropylamino chain at the condensed heterocyclic ring mimics the morpholine group of several triazine derivatives. Higher-resolution images are available in the Supporting Information.

with a 3-F in nitro or inverted amide derivatives (**4g**–**h** and **7a**–**b**, respectively). Moreover, replacement of the rhodanine scaffold of **4a** with a succinic moiety resulted in **11** with lower activity. To overcome the intrinsic limitations possibly affecting the pharmacophoric model generated by the software LigandScout[23] used to identify **4a**, a high-throughput docking approach (HTD, as described in the Experimental Section below) was applied to the Asinex Gold collection.[14a] As a result, the triazine derivative **15a**, endowed with submicromolar activity (0.4 μM, Table 2), was identified. The best ranked interaction mode within the ATP binding site of DDX3 showed the indolinone moiety within a network of hydrogen bonds with amino acid residues constituting the left pocket (Figure 1D). In particular, the carbonyl group of the ligand interacted with the terminal portion of the Gln207 side chain, mimicking the carbonyl group of the rhodanine nucleus. Moreover, the NH of the lactam group was a hydrogen bond donor for the carbonyl moiety of Arg202. It is important to note that the hydrogen bond acceptor-donor motif involving Arg202 and Gln207 was conserved in the X-ray crystal structure of DDX3, where the adenine moiety of the nucleotide made two hydrogen bonds with the same residues. The heterocyclic portion of the indoline nucleus also interacted with Tyr200 (in a similar way already found for the rhodanine ring), while the condensed phenyl ring was located within the large cavity (the left pocket) where the bromophenyl moiety of **4a** was accommodated. An additional hydrogen bond was found between one of the anilino NH groups and the carbonyl moiety of Gly227 within the upper pocket. Hydrophobic contacts between the second anilino moiety and Thr231, Ile282, Ala232, Gln281, and the alkyl spacer of Glu285 were also found. A focused library of structural analogues of **15a** was synthesized, while additional derivatives were purchased from commercial sources to find compounds with better activity with respect to the parent hit (Table 2). Removing the hydrogen bond donor group by replacement of the anilino moiety of **15a** with a morpholine led to the inactive derivative **15b**. Computational results suggested that **15b** could be located within the enzyme binding site in a different orientation from that of **15a**. In fact, the indoline nucleus occupied the right pocket and interacted by hydrogen bonding with Gln281, whereas the morpholino ring was accommodated within a region exposed to the solvent, thus lacking the hydrogen bond with Gly227 found for **15a**. Finally, the anilino moiety was found within the left pocket previously occupied by the indolinone nucleus of **15a** (Figure 1E). The lack of the hydrogen bond donor-acceptor motif similar to that exhibited by the adenine portion of the natural ligand and the inability of the morpho-

Table 2. Structures and biological data for the new triazine derivatives.

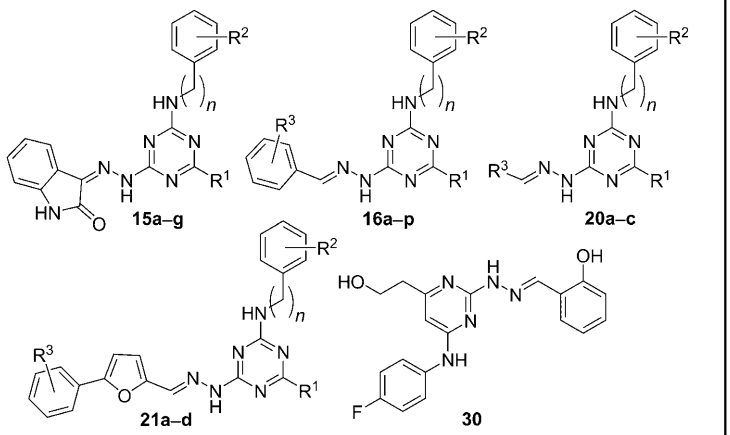

Compd	*n*	R^1	R^2	R^3	K_i[a] [μM]
15a[b]	0	NH-Ph	H	–	0.4
15b[b]	0	morpholinyl	H	–	NA
15c[b]	0	morpholinyl	3-Cl	–	1.6
15d[b]	0	morpholinyl	3-Cl, 4-Me	–	3.2
15e	1	morpholinyl	H	–	NA
15f	1	morpholinyl	3-Cl	–	2.9
15g	1	NEt_2	H	–	0.1
16a[b]	0	NH-Ph	H	2,4-OH	33
16b[b]	0	NH-Ph	H	3,4-diCl	18
16c[b]	0	NH-Ph	H	3-NO_2, 4-OH	7.5
16d[b]	0	NH-Ph	H	4-Br	NA
16e[b]	0	NH-Ph	H	4-$NHCOCH_3$	0.3
16f[b]	1	NH-Ph	H	4-$NHCOCH_3$	0.5
16g[b]	0	morpholinyl	H	4-$NHCOCH_3$	2.2
16h[b]	0	morpholinyl	3-Cl, 4-Me	2-OH	1.6
16i	1	morpholinyl	4-F	2-OH	0.7
16j	1	morpholinyl	H	2-OH	0.6
16k[b]	1	morpholinyl	H	2-OH, 5-Cl	1.9
16l[b]	1	morpholinyl	H	2-OH, 3-NO_2	4.0
16m	0	morpholinyl	4-F	2-OH	0.4
16n	0	NH-Ph(4-F)	4-F	2-OH	0.1
16o	1	morpholinyl	3-Cl	2-OH	62
16p	1	NEt_2	H	2-OH	0.5
20a[b]	0	morpholinyl	4-F	2-methyl-indol-3-yl	0.2
20b	0	morpholinyl	4-F	1-naphthyl	86
20c	0	morpholinyl	4-F	2-naphthyl	8.5
21a[b]	0	morpholinyl	4-F	2-Cl, 4-NO_2	0.3
21b[b]	0	morpholinyl	4-F	2-Cl, 5-NO_2	3.6
21c[b]	0	morpholinyl	H	2-Cl	3.2
21d[b]	0	piperidinyl	H	4-Cl	0.4
30	–	–	–	–	9.0

[a] Apparent equilibrium dissociation constant for the inhibitor to the target enzyme DDX3. [b] Purchased from Asinex.

line ring to make the additional hydrogen bond contact with Gly 227 seemed to be responsible for the dramatic decrease in activity of unsubstituted morpholino derivatives **15b** and **15e**. A significant activity was restored by introduction of a chloride substituent at position 3 (**15c**, **15d**, and **15f**, Figure 1F) that was accommodated within a best interaction region of the left pocket, as identified by GRID software for the chloride probe. The same trend in activity was found for compounds bearing a benzylamino side chain instead of the anilino substituent (**15e** and **15f**).

Opening the indolinone ring of **15a** into a benzylidenehydrazine chain resulted in a significant decrease in activity (**16a–d**; 33, 18, and 7.5 μM or no activity, respectively), independently from the substituents at position R^3. The sole exception was represented by the acetamido derivatives **16e–g** that restored a micromolar or submicromolar activity. Such compounds restored the hydrogen bond with Gly 227 of the upper pocket and maintained the hydrogen bonds involving their NH amide group and Gln 281. This contact was disrupted by transformation of the acetamido terminus into hydroxy or halogen substituents, as in **16a–d** (Figure 2A). Compound **16g**, although being able to maintain contacts mediated by its acetamido group, was less active than **16e** because of its inability to interact with Gly 227 of the upper pocket by means of one of its anilino moieties.

The benzylidene derivative **16h** showed an activity similar to that of the corresponding indolinone analogue **15d** (1.6 vs. 3.2 μM, respectively), accounted by a very similar interaction pattern with the binding site (Figure 2B). The 3-Cl and 4-Me substituents of these compounds were accdommodated within minimum point regions of the left pocket found by GRID for the chloride and methyl probes, respectively, while the phenyl ring was at the right distance for a possible π–π interaction with the aromatic portion of Tyr 200.

Keeping fixed the morpholine and the 2-OH group at R^1 and R^3, respectively, the activity was neither affected by decreasing the size of the substituent at R^2 (**16i**), by eliminating it (**16j–l**), nor by shortening of the benzylamino chain of **16i** to the anilino moiety of **16m**. Docking simulations showed that the 2-OH group of **16m** and **16i** was located within the right pocket and interacted with the protein by means of the same hydrogen bonds already found for **4a**, while the fluorine atom on their anilino or benzylamino groups occupied a region where electron-rich substituents are preferred and where an additional minimum interaction point (-3.49 kcal mol^{-1}) was found for the fluorine probe. The same region also accommodated the fluoro substituent of **16n**. These results also explained the fact that a benzylamino chain instead of an anilino group (**16i** and **16m**) did not affect activity. Transforming the morpholino moiety of **16j** into the diethylamino side chain of **16p** did not influence the activity, contrarily to that found for **15e** and **15g**.

Finally, replacement of the phenolic moiety of **16m** with an indole nucleus (**20a**) retained a micromolar activity, while bulkier susbtituents (1- and 2-naphthyl) led to **20b** and **20c** with an activity of 86 and 8.5 μM, respectively. The 2-naphthyl ring showed hydrophobic contacts with a lipophilic region defined by Thr 226, Lys 230, Leu 278, and Phe 234, where GRID found several minimum points for a C3 (methyl) probe, while its 4-F substituent was located within the minimum energy point for

the fluoride at the left pocket (Figure 2D). However, changing the substitution pattern of the naphthyl ring was detrimental for activity because of steric clashes found for the 1-naphthyl analogue **20b**.

When the condensed nucleus was replaced by a phenylfuranyl chain as in **21a**, activity was restored at the micromolar concentration. The chloro and nitro substituents of **21a** were found within minimum energy regions identified by GRID for the corresponding probes (Figure 2E). Consequently, changing the substitution pattern (**21b**) or eliminating the nitro group (**21c**) caused a decrease in activity of about one order of magnitude. In fact, the 2-chloro substituent of **21b** occupied a minimum region for the chloride different from and less profitable than that found for the 2-Cl group of **21a**, thus explaining the lower activity. Simplification of the morpholine into a piperidine as in **21d** resulted in a good activity (0.4 μM), although it is not possible to assess the individual impact of these two simultaneous changes (i.e., morpholino vs. piperidino and 2-Cl vs. 4-Cl) on activity.

Taking into account the above described pharmacophoric interactions with the ATP binding pocket of DDX3, we tried to introduce such key features into a different scaffold. Among the designed compounds, the pyrimidine derivative **30** was synthesized and showed an activity (9.0 μM) similar to that of **4a** (5.4 μM) and **16h** (1.6 μM). It had an interaction pattern similar to that of AMP, with hydrogen bond interactions involving the left and right pockets (residues Arg202, Lys230, and Thr231, respectively), a possible π–π interaction with Tyr200 and additional hydrogen bond contacts with Glu285 and Tyr200. However, the loss of important hydrophobic interactions with the right pocket accounts for its activity being lower than that of similar triazine analogues, such as **16m**. The pyrimidine derivative **30** represents, however, a promising hit for future optimization.

Finally, considering the lower toxicity profile of the rhodanine derivatives (**4a** and **4b**, Table 3) relative to the triazine derivatives (**16e**, **16m**,**n**, and **20a**, Table 3), we focused our attention on the first class of compounds in the attempt to identify analogues endowed with an improved selectivity index. Based on the synthetic approach reported in Scheme 2, a virtual library of substituted rhodanines was designed using the software SmiLib v2.0.[24] In particular, a series of aldehydes and primary amines available in our stockroom, were combined to generate ~16000 virtual compounds. The library was then submitted to a virtual screening protocol with the aim of identifying compounds characterized by a predicted affinity for the ATP binding pocket and an aqueous solubility (QP LogS - conformation independent) better than that of **4a**. Compound **31** was classified as the best ranked entry and purchased from commercial sources. Docking simulations showed that its pose within the ATP-binding site (Figure 2F) was reminiscent, at the same time, of the binding mode of both rhodanine and morpholino-triazine derivatives, such as **4a** and **15f** (Figure 1A and Figure 1F, respectively). In fact, the phenylethyl-rhodanine moiety of **31** resembled the left molecular portion of rhodanine derivatives **4**, and the hydroxypropylamino chain mimicked the morpholino moiety and interacted with Lys288, as the morpholine oxygen of triazine derivatives did. Finally, the carbonyl group of the condensed heterocycle was able to make hydrogen bond contacts already found for the 2-OH group of **4a** (Figure 1A) and **16h** (Figure 2B). Biological evaluation of **31** resulted in good antienzymatic (Table 1) and antiviral activity (Table 3), with a selectivity index higher than 10.

Table 3. Cytotoxicity and antiviral activity of DDX3 inhibitors.

Compd	EC_{50}[a] [μM]	CC_{50}[b] [μM]			SI[c]		
		HeLa	MOLT-4	PBMCs	HeLa	MOLT-4	PBMCs
4a	83±7	200	200	150	2.4	2.4	1.8
4b	7.5±0.7	50±5	50±10	50±5	6.7	6.7	6.7
4l	–	7.5±0.5	–	–	–	–	–
4t	–	10±1	–	–	–	–	–
15c	–	7.5±0.7	–	–	–	–	–
15d	–	7.5±0.5	–	–	–	–	–
15f	–	20±3	–	–	–	–	–
15g	–	5±1	–	–	–	–	–
16b	–	100±10	–	–	–	–	–
16e	10±1	20±2	15±2	40±6	2.0	1.5	4.0
16g	–	20±2	–	–	–	–	–
16h	–	20±2	–	–	–	–	–
16i	–	7.5±0.5	–	–	–	–	–
16j	–	10±1	–	–	–	–	–
16k	–	10±1	–	–	–	–	–
16l	–	20±2	–	–	–	–	–
16m	2.5±0.1	2.5±0.3	5±1	10±1	1.0	2.0	4.0
16n	2.0±0.2	20±2	10±1	8.0±0.5	10	5.0	4.0
16p	–	5±1					
20a	4.0±0.5	25±3	20±2	15±2	6.3	5	3.7
21b	–	7.5±0.7	–	–	–	–	–
21c	–	7.5±0.7	–	–	–	–	–
21d	–	20±3	–	–	–	–	–
4c	–	>50	ND[d]	>50	–	–	–
4s	–	>50	ND	>50	–	–	–
15a	–	17.9	ND	15.0	–	–	–
16f	–	>50	ND	21.4	–	–	–
21a	–	4.7	ND	11.7	–	–	–
31	6.5±0.7	65±5	ND	70±7	10	–	10.7

[a] Toward HIV-1, the micromolar concentration required to suppress 50% of HIV-1 proliferation. [b] The micromolar concentration required to suppress 50% of cell viability. [c] Selectivity index: the ratio of cytotoxicity (CC_{50}) to antiviral activity (EC_{50}). [d] ND: not determined.

Antiviral activity of second-generation DDX3 inhibitors

The first-generation DDX3 inhibitor **4a** displayed very low cytotoxicity on HeLa cells ($CC_{50} > 200$ μM) but only modest anti-HIV activity ($EC_{50} = 83$ μM, Table 3). Figure 3A shows the antiviral activity of **4a** on PBMCs infected with HIV-1 in comparison with the most potent second-generation derivatives **4b**, **16e**, **16m**, **16n** and **20a**. It can be appreciated that the last compounds showed between 40 and 60% decrease in viral load already at 3 μM, while **4a** had to be added at 50 μM to show similar effects. Dose–response curves were generated for **4a** and **16n**. As shown in Figure 3B, **16n** showed a 41-fold higher antiviral potency on PBMCs infected with HIV-1 ($EC_{50} = 2$ μM) than the protoype DDX3 inhibitor **4a**. Similar curves yielded EC_{50} values of 7.5, 10, 2.5, and 4.0 μM, respectively, for **4b**, **16e**, **16m**, and **20a**. To evaluate the specificity of action, the most active compound **16n** was tested against different ATP-hydrolysing enzymes (Table 4). Compound **16n** showed no activity toward T4 PNK, HCV NS3 ATPase/helicase, and c-Src human tyrosine kinase up to 100 μM. When tested against another member of the DDX family of ATPase/helicases, DDX1, compound **16n** proved to be 500-fold less active than its activity against DDX3, further confirming its high selectivity for the desired target.

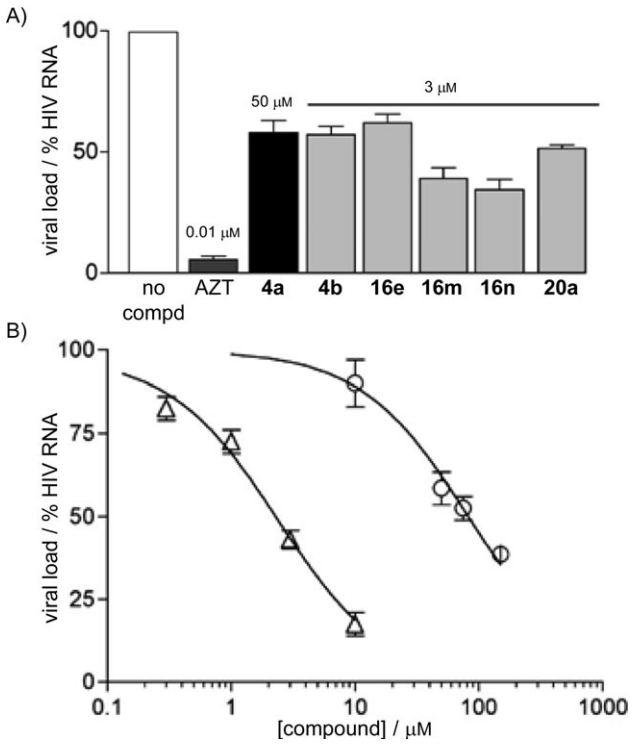

Figure 3. Antiviral activity of DDX3 inhibitors. A) Comparison of the antiviral activity (expressed as percent viral RNA relative to control) on infected PBMCs of a fixed dose of selected inhibitors. Measurements were performed at 72 h post-infection. Values are the means plus SD of three independent replicates. White bar: control without drugs; dark-grey bar: postive control with AZT (0.01 μM); black bar: first-generation inhibitor **4a** (50 μM); light-grey bars: second-generation DDX3 inhibitors **4a**, **4b**, **16e**, **16m**, **16n**, and **20a** (3 μM). B) Dose–response curves for the inhibiton of HIV-1 replication (expressed as percent viral RNA relative to control) in infected PBMCs by **4a** (○, $EC_{50} = 83 \pm 7$ μM) and **16n** (△, $EC_{50} = 2 \pm 0.2$ μM). Measurements were performed at 72 h post-infection. Values are the means ± SD of three independent replicates.

Table 4. Selectivity of inhibitor **16n** toward various ATP-hydrolysing enzymes.

Enzyme[a]	K_i[b] [μM]	Selectivity
T4 PNK	>100	>1000
HCV NS3	>100	>1000
c-Src	>100	>1000
DDX1	49 ± 4	490
DDX3	0.1 ± 1	1

[a] T4 PNK: phage T4 polynucleotide kinase, HCV NS3: human hepatitis C virus NS3 ATPase/RNA helicase, c-Src: human Src tyrosine kinase, DDX1: human ATPase/RNA helicase DDX1, DDX3: human ATPase/RNA helicase DDX3. [b] Values are the mean of three independent measurements; assays were carried out as described in the Experimental Section.

Cytotoxicity studies on second-generation DDX3 inhibitors

Selected compounds were also tested against the HeLa cell line for their cytotoxic activity. Cell viability was measured using the MTS-based CellTiter assay. CC_{50} values (dose required to suppress 50% of cell viability) varied significantly among the considered compounds (Table 3), with several molecules (**4a**, **4b**, and **16b**) displaying very low cytoxicity ($CC_{50} >$ 50 μM), while others were endowed with potent antiproliferative activity ($CC_{50} \leq 5$ μM). There was no clear correlation between the cytotoxic and antienzymatic potencies: for example, compounds **4b** and **16m** display almost equal potencies against DDX3, but **16m** is 20-fold more toxic than **4b**.

These data suggest that cytoxicity and antienzymatic activities could, in principle, be uncoupled through chemical modifications of the pharmacophore. Cytotoxicity of compounds endowed with the highest anti-HIV activity (**4a**, **4b**, **16e**, **16m**, **16n**, **20a**, and **31**) was also evaluated on two additional cell types: the T-lymphocytic MOLT-4 cell line and the primary PBMCs used for the anti-HIV assays (Table 3). Values of the selectivity index (defined as the ratio PBMC CC_{50}/HIV EC_{50}) for **4b**, **16e**, **16m**, **16n**, and **20a** on PBMCs were 6.7, 4.0, 4.0, 4.0, and 3.7, respectively, clearly indicating that the relative cytotoxicity was still an important issue limiting the efficacy of these compounds. The gain in antiviral activity obtained by the synthesis of **4b**, **16e**, and **16n** (HIV EC_{50} ranging from 8- to 41-fold better with respect to first-generation compound **4a**) was only about twofold higher than the corresponding increase in cytotoxicity (CC_{50} from 5- to 20-fold). Thus, SAR studies were conducted in order to improve the selectivity of our inhibitors: compound **31**, identified out of a library of ~16000 virtual compounds, showed a good antienzymatic and antiviral activity with a selectivity index higher than 10 (Table 1 and Table 3).

Effect of DDX3 knockdown on cell growth

Because optimized compounds all showed some degree of cytotoxicity, we revisited the target. Validating a cellular enzyme

as a potential antiviral target requires a precise knowledge of the potentially negative effects of its inhibition at the host cell level. Since the first report of DDX3 as a cofactor for HIV-1 replication, studies addressing the consequences of its knockdown in human cells have led to conflicting results. To implement a rigorous knowledge-based approach for the understanding and improvement of the toxicity profile of our compounds, we have set up a carefully controlled cellular system to examine the effects of DDX3 knockdown in HeLaCCR5 cells on cell growth and viral replication.

Stable DDX3 knockdown HeLaCCR5 cell lines were generated using a lentiviral vector expressing two copies of specific microRNA targeting DDX3. As a control, a vector with four specific mismatch mutations in the hairpins was generated. As shown in Figure 4, the polyclonal knockdown cell line showed

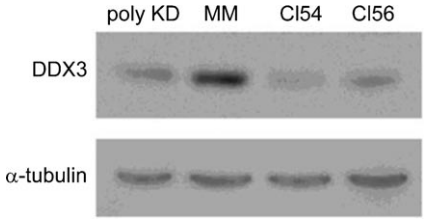

Figure 4. Western blot analysis of DDX3 knockdown cell lines. Stable DDX3 knockdown HeLaCCR5 cell lines were generated using lentiviral vector technology. DDX3 levels in the polyclonal knockdown cell lines (poly KD), the mismatch control cell line (MM), and the two strongest monoclonal cell lines (Cl54 and Cl56) were analysed by Western blot using an anti-DDX3 antibody. Equal loading was controlled by α-tubulin detection.

at least 50% knockdown relative to the mismatch control. Morevoer, monoclonal cell lines were derived to achieve a better knockdown. Among the two best cell lines (clones 54 and 56), clone 54 showed ~75% knockdown relative to the mismatch.

Evaluation of the cellular phenotype in DDX3 knockdown cells

Following stable suppression of DDX3, the cellular phenotype was studied with respect to proliferation potential. Equal numbers of the mismatch, polyclonal, and monoclonal DDX3 knockdown cells were seeded and cell growth was monitored over time. As shown in Figure 5, knockdown of DDX3 did not affect cell growth. Because the knockdown was not complete, these results at least indicated that low levels (25% of normal) of DDX3 might be sufficient to sustain cell growth. While Lee and co-workers[25] reported a strong effect on cell viability upon siRNA-mediated DDX3 knockdown in HeLa cells and *Drosophila* cells, our results confirm the observations of Ishaq and co-workers.[8]

Effect of DDX3 knockdown on the HIV-1 RRE-Rev viral RNA export pathway

Having established a stable cell line effectively depleting DDX3, we used it as a tool to re-investigate the role of DDX3

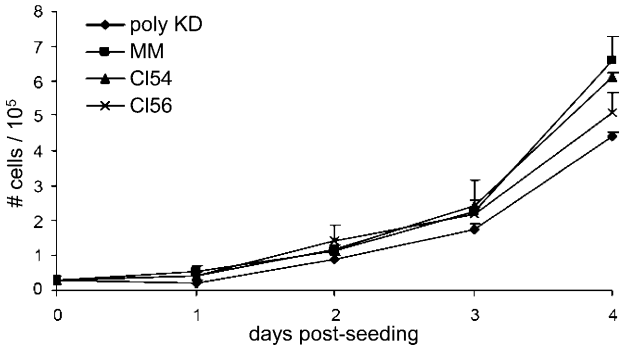

Figure 5. Effect of DDX3 knockdown on cell growth. For growth curve analysis, 50000 cells of the polyclonal knockdown cell line (poly KD), the mismatch control cell line (MM), and the two monoclonal cell lines (Cl54 and Cl56) were seeded at day zero in a 24-well plate. Cell growth was monitored by counting the cells at the indicated time points. Values are the mean of triplicate measurements in a representative experiment. Error bars represent the corresponding standard deviations. The experiment was performed twice.

in HIV-1 replication, as part of our target validation process. In the initial report on DDX3[10] the effect on HIV-1 was analysed in a reporter system measuring Rev-mediated viral RNA (vRNA) export. In this assay, a CMV-driven HIV-1 gag–pol construct containing an HIV-1 Rev response element (RRE) sequence (Figure 6A) was co-transfected with a HIV-1 Rev expression construct. Upon expression, Rev binds to the RRE enabling export of non-spliced gag–pol coding vRNA. This results in gag-derived p24 expression which can be measured in the supernatant. The same construct with a CTE (Mason-Pfizer monkey virus constitutive transport element) instead of an RRE was used as a control. Although much less active, this CTE enables Rev-independent mRNA export.

This assay was used to evaluate the effect of DDX3 knockdown on the RRE-Rev axis in the DDX3 knockdown cell lines (Figure 6). Although we could not observe an effect in the polyclonal cell lines in comparison with the mismatch control, the monoclonal cell lines showed a 3- to 10-fold defect in p24 production. Expression of the gag–pol RRE construct in the absence of Rev did not result in detectable levels of p24. In addition, as a control, a plasmid encoding eGFP driven by the CMV promoter was co-transfected. No significant difference in eGFP expression was observed excluding effects on expression or Rev-independent mRNA export (results not shown). These results confirm the previously published results[10] and corroborate the involvement of DDX3 in the RRE-Rev axis.

Effects of DDX3 knockdown on virus production

If DDX3 is indeed essential for the RRE-Rev axis, knockdown of DDX3 should hamper virus production. To test this hypothesis, HeLaCCR5 DDX3 knockdown cells were transfected with a HIV-1_{NL4-3} molecular clone. The p24 content of the supernatant was measured 48 h post transfection and compared with the mismatch cell line (Figure 7). A twofold decrease in p24 production could be observed in the DDX3 knockdown cell lines. This effect was less significant than that obtained by Yedavalli and

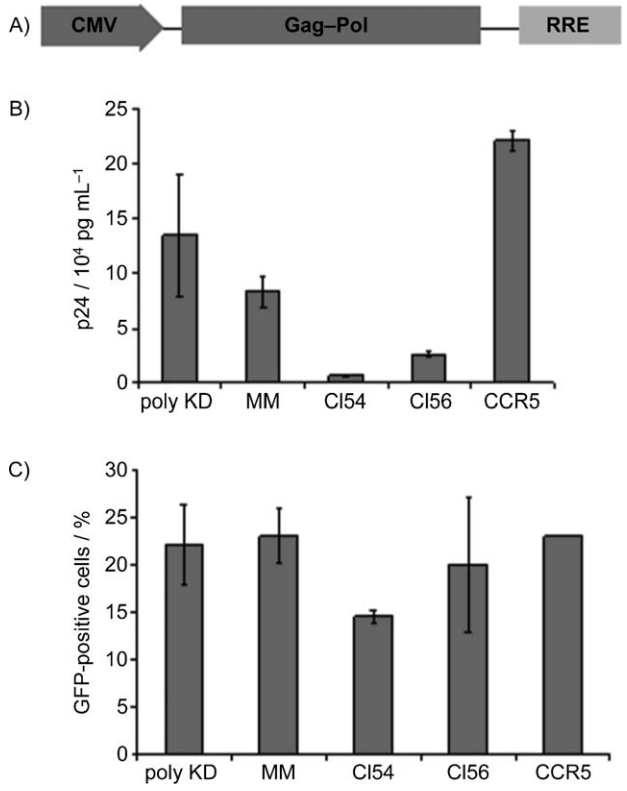

Figure 6. Role of DDX3 in the Rev-RRE mRNA export axis. A) Schematic representation of the Rev reporter system. To measure Rev-dependent mRNA export, the reporter plasmid was co-transfected with pcRev and a plasmid encoding eGFP to control for transfection efficiency. The amount of p24 in the supernatant was measured 48 h post-transfection. B), C) The different HeLaCCR5-derived DDX3 knockdown cell lines (poly KD and monoclonal 54 and 56) were cotransfected with the gag–pol RRE reporter construct and a Rev and eGFP expression plasmid. Panel B shows the p24 content in the supernatant 48 h post-transfection. Panel C shows the eGFP transfection efficiency as measured by FACS analysis. Values are the mean of triplicate measurements in a representative experiment. The experiment was performed twice. Error bars represent the corresponding standard deviations.

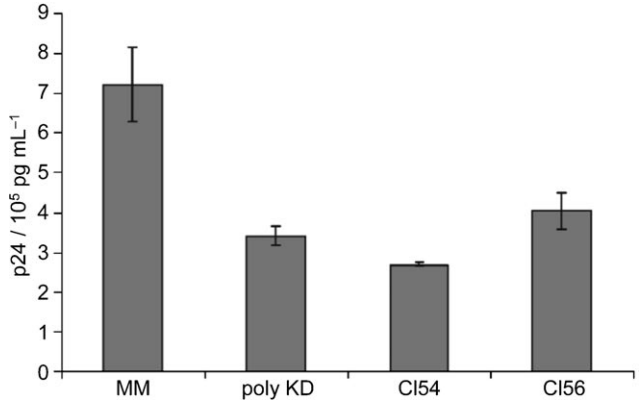

Figure 7. Effect of DDX3 knockdown on virus production. HeLaCCR5 DDX3 polyclonal knockdown cells and the monoclonal derived cells (clone 54 and 56) were transfected with a HIV_{NL4-3} molecular clone. The p24 content of the supernatant was measured 48 h post-transfection and compared with the mismatch (MM) cell line. Values are the mean of two measurements in a representative experiment. Error bars represent the corresponding standard deviations. The experiment was done twice.

co-workers.[10] Possibly, the knockdown in our cell lines might not be strong enough to detect a more pronounced replication defect. In this regard, Yedavalli[10] obtained a stronger knockdown and a stronger defect in the Rev reporter system. However, our data collectively confirm a role of DDX3 in the HIV-1 replication cycle, thus validating it as a novel anti-HIV target. We cannot exclude that the toxicity of our compounds might be, at least in part, also due to targeting other DEAD-box helicases. For the future design of more specific DDX3 inhibitors, starting from the most active compounds identified here, we are now conducting a counterscreening for lack of inhibition of other helicases, such as DDX1.

Conclusions

The problem of drug resistance development due to mutations in HIV-1 proteins targeted by antiviral drugs could be overcome by the development of novel anti-HIV agents targeting host factors essential for viral replication. One of such host factors is the DEAD-box RNA helicase/ATPase DDX3.[5,8,10,11,15] Here we report a rational drug design and full characterization of second-generation DDX3 inhibitors endowed with nanomolar antienzymatic activity in vitro and low-micromolar anti-HIV activity in infected cells. In addition, we have conducted a thorough analysis that confirmed DDX3 as a valid anti-HIV target. The compounds described here represent a significant advancement in the quest of potential novel drugs targeting HIV-1 host cofactors. The observed toxicity is still significant, but the results presented in this work support the possibility to design more specific DDX3 inhibitors as effective anti-HIV agents.

Experimental Section

Biology

Enzymatic assays: Recombinant His-tagged human DDX3 was expressed in *E. coli* and purified as described.[12] ATPase activity was tested with a luciferase-based luminescence assay (easylite-Kinase, PerkinElmer) on 96-well microtiter plates as described.[11] Briefly, recombinant purified human DDX3 (50–100 ng) was incubated in a 15 μL total reaction volume with reaction buffer (25 mM Tris-HCl, pH 7.5, 5 mM $MgCl_2$), in the presence of increasing amounts of ATP and/or different combinations of ATP and the inhibitor to be tested. Reference curves in the absence of inhibitor (giving the 100% of enzymatic activity) and in the absence of enzyme (giving the baseline), were also included in each experiment. Reading was performed with a Microbeta Trilux (PerkinElmer) luminometer, according to the manufacturer's protocol. T4 PNK (OptiKinase) was from USB Corp. (Cleveland, OH, USA). Activity was assayed according to the manufacturer's protocol in the absence or presence of increasing amounts of **16n**. HCV NS3 was purified and its ATPase activity assayed as described[26] in the absence or presence of increasing amounts of **16n**. Human c-Src was purchased from Upstate (Lake Placid, NY, USA). Activity was assayed as described[27] in the absence or presence of increasing amounts of **16n**. The cDNA for human DDX1 was kindly provided by Dr. U. Dietrich (Georg-Speyer-Haus, Institute of Biomedical Research, Frankfurt, Germany). Human DDX1 was cloned from human PBMCs and purified as de-

scribed above for DDX3. DDX1 ATPase activity was tested under the same conditions used for DDX3, in the absence or presence of increasing amounts of **16n**.

Kinetic analysis: To determine the inhibitory constant (K_i), ATPase reactions were performed as described, in the presence of increasing amounts of inhibitor and variable ATP concentrations. Variations of the initial velocities of the reaction as a function of ATP concentrations in the absence or presence of inhibitors were analysed with Equation (1), in which k_{cat} is the reaction rate, E_0 is the input enzyme concentration, [ATP] is the variable substrate concentration, and K_S is the apparent affinity for the substrate. $K_S = K_M$ in the absence of the inhibitor, whereas $K_S = K_{M(app)}$ in the presence of the inhibitor.

$$K_i = k_{cat}E_0/\{1 + (K_S/[ATP])\} \quad (1)$$

Variations of the percent inhibition as a function of compound concentrations at different ATP concentrations were fitted to the equation for cooperative binding:

$$\%\ \text{inhibition} = V_{max}[I]^n/(K_i + [I]^n) \quad (2)$$

for which V_{max} is the apparent maximal rate of the reaction in the absence of the inhibitor, [I] is the variable inhibitor concentration, n is the cooperativity index, and K_i is the apparent inhibition constant.

Antiviral assays: The susceptibility of HIV-1 recombinant strains to drugs was performed as previously reported.[28] In brief, 0.5 μg of each HIV-1 plasmid construct was transfected into $CD4^+$ HeLa cells by using the Lipofectin Transfection Reagent (Invitrogen, Groningen, The Netherlands) according to the recommendations of the manufacturer. After 3 days of incubation at 37 °C, the cell supernatants, which contained reconstituted viable recombinant viruses, were collected. Quantification of the newly produced recombinant strains was done by determination of the HIV RNA copy number in the cell culture supernatants. In detail, transfected HeLa $CD4^+$ cell culture supernatants containing 1×10^9 RNA copies mL^{-1} were used to infect aliquots of 20×10^6 phytohemagglutinin-stimulated peripheral blood mononuclear cells (PBMCs) obtained from HIV-seronegative blood donors. After 4 h of incubation, supernatants were removed and infected PBMCs were incubated at 37 °C in 10 mL of RPMI 1640 medium (Eurobio, Les Ulis Cedex B, France) supplemented with 20% fetal calf serum (Life Technologies, Ltd., Paisley, UK), 2 mM L-glutamine, 100 U mL^{-1} penicillin, 100 μg mL^{-1} streptomycin, 50 U mL^{-1} interleukin-2 (Roche Diagnostics, Mannheim, Germany), 5 μg mL^{-1} hydrocortisone (Sigma Chemical Co., St. Louis, MO, USA), and with fourfold dilutions of antiretroviral drugs. A no-drug control for each drug dilution was included in each assay. The HIV-1 RNA level in the cell culture supernatant was quantified at 72 h post-infection. Recombinant HIV-1 strains from treatment-naive patients and multidrug resistance-associated changes were assayed in parallel. The degree of inhibition of viral replication was measured by determining the HIV-1 RNA level in the supernatants of cell cultures and was expressed as the fold increase in the 50% inhibitory concentration (IC_{50}) for resistant recombinant HIV-1 variants, compared with the IC_{50} for the wild-type recombinant variant. Each test was performed in triplicate.

Cytotoxicity assays: Compounds were tested against the human cervical cancer cell line HeLa, the human T-lymphocytic leukemia cell line MOLT-4, and human primary PBMCs. Increasing doses of the compounds to be tested were added to 2×10^6 cells. Culture medium supplemented with fresh compound was replaced every 24 h. After 72 h of continuous exposure of the cells to the compounds at 37 °C, cell viability was measured with the CellTiter 96 (Promega) viability assay, which contains MTS [3-(4,5-dimethylthiazol-2-yl)-5-(3-carboxymethoxyphenyl)-2-(4-sulfophenyl)-2*H*-tetrazolium, inner salt] and an electron coupling reagent (phenazine ethosulfate). Assays were performed by adding 20 μL of the CellTiter 96 reagent directly to culture wells, followed by incubation for 4 h and subsequent absorbance measurement at 490 nm with a 96-well plate reader. The quantity of formazan product as measured by the amount of 490 nm absorbance is directly proportional to the number of living cells in culture. Determinations for each compound dose were done in quadruplicate. The CC_{50} values were calculated from dose–response curves using the mean values of each set of determinations.

Plasmids and vector production: pcRev was a kind gift from M. Malim (London, UK). pCMV NL gag–pol RRE was a kind gift from E. Freed (Frederick, MD). Lentiviral vectors encoding DDX3 microRNA were essentially cloned as described before.[29,30] The DDX3 target sequence was 5′-GAG GAA CAT AAA TAT TAC TAA-3′. As a mismatch control, the sequence 5′-GAG GAA CAT ATT ATT TAC TAA-3′ was used. Lentiviral vectors were prepared as described previously.[31]

Cell culture and generation of DDX3 knockdown cells: HeLaP4-CCR5 cells (a gift from P. Charneau, Paris, France) were grown in Dulbecco's modified Eagle's medium (Gibco-BRL, Merelbeke, Belgium) supplemented with 10% fetal calf serum (Sigma, Bornem, Belgium) and 20 μg mL^{-1} gentamicin (Gibco-BRL) at 37 °C and 5% CO_2 in a humidified atmosphere. To generate the DDX3 knockdown and control cells, cells were transduced with the DDX3 microRNA encoding lentiviral vector or mismatch control vector and selected with zeocin (200 μg mL^{-1}; Invitrogen, Merelbeke, Belgium).

Western blot analysis: SDS (1%) protein extracts were separated by sodium dodecyl sulfate-polyacrylamide gel electrophoresis. DDX3 was detected using a DDX3 antibody (Imtec, Belgium). Equal loading was controlled by α-tubulin detection using anti-α-tubulin antibody (Sigma, Belgium). Proteins were visualized by chemiluminescence (ECL Plus; Amersham Biosciences, Uppsala, Sweden).

Analysis of DDX3 knockdown cells: To analyse the effect of DDX3 on the RRE-rev axis, 100000 cells per well of the respective cell lines were plated in a 24-well plate. At 24 h post-seeding, cells were transfected with 1 μg pCMV NL gag–pol RRE, 0.5 μg pcRev, and 0.5 μg peGFP-C1. Forty-eight hours later, p24 content in the supernatant was measured using the Alliance HIV-1 P24 ANTIGEN ELISA Kit (PerkinElmer, Zaventem, Belgium), and eGFP expression was analysed by FACS. To analyse viral production, cells were transfected with pNL4-3 (NIH AIDS Research and Reference Reagent Program) and analysed for p24 content at 48 h post-transfection.

Computational methods

The structure-based pharmacophore modeling and molecular docking protocol that was used to identify **4a** was previously described.[11] In brief, the pharmacophore was generated by means of LigandScout, a software able to codify the crucial interactions between DDX3 and the natural ligand AMP (in the pdb complex coded as 2I4I) into pharmacophoric features.

Importantly, a kinetic characterization of **4a** suggested it as an uncompetitive inhibitor. Considering that uncompetitive inhibition occurs when the inhibitor binds only in the presence of ATP and that DDX3 may act as a multimeric enzyme, **4a** could bind in the ATP binding site of one or more monomers of the multimeric DDX3 complex, while ATP binds to the other monomers. As this

model was consistent with the observed kinetic behavior of **4a**, we chose to dock the new compounds within the ATP binding site of a DDX3 monomer. However, we are aware of the fact that an alternative binding mode for the new compounds could be based on DDX3 sites that are different from the ATP binding pocket.

The model resulting from LigandScout was exported to Catalyst software[32] and then used as a three-dimensional query to perform a search within a database of commercially available compounds. In particular, the Asinex Gold and Synergy databases were downloaded from the web and converted into a multiconformer database by means of the *cat*DB command of Catalyst (FAST method, 250 as the maximum number of conformations for each entry). Catalyst was also applied to filter the database with the model (fast flexible search routine), keeping as putative hits all the database entries with a fit value higher than 1.00. The resulting compounds were exported to Cerius2 (version 4.10L)[33] to calculate their physicochemical properties and remove entries unable to satisfy Lipinski's rule of five, thus leading to 70 entries. They were submitted to docking simulations and scoring, allowing us to choose 10 compounds including **4a**.

In a different approach, to overcome the intrinsic limitations affecting the structure-based pharmacophoric model, a virtual screening protocol based on a high-throughput docking approach (HTD) was also applied to the Asinex database in an attempt to find additional small molecules able to bind the ATP binding site of DDX3. A rule-based approach was applied to enumerate all the plausible alternative tautomeric forms of each database entry, that were in turn docked into the DDX3 binding site by means of the GOLD software. Considering that no known small molecules able to bind the ATP pocket of DDX3 are currently available, the reliability of the docking approach and the performance of the scoring function in finding active entries within a database cannot be checked a priori. The only way to validate the entire virtual screening protocol was through the identification of putative hit compounds and their submission to biological evaluation. On the basis of this considerations and taking into account that the DDX3 ATP binding site showed either hydrophobic clefts or residues with hydrogen bond capabilities, both the scoring functions of GOLD were applied: GoldScore usually recommended to score ligand binding mainly based on hydrogen bond contacts, and ChemScore preferred for evaluating interactions mainly attributable to hydrophobic groups and residues. Default settings of the GOLD genetic algorithm were applied.

The subunit of DDX3 complexed with the ligand AMP was extracted from the entire crystallographic structure 2I4I and submitted to a preliminary structural optimization to avoid any possible steric clash between the ligand and the protein (MacroModel software,[34] OPLS_2005 force field,[35] Polak–Ribiere conjugate gradient, and a 100 kJ mol^{-1} Å^{-2} as a constraint constant applied to backbone atom; 0.01 kJ Å^{-1} mol^{-1} as the energy gradient root mean square to converge). The region included in a 10 Å shell from AMP was included in docking calculations. For each ligand, 100 independent genetic algorithm (GA) runs were performed, with a maximum of 100 000 GA operations on a set of five islands with a population size of 200 individuals. The remaining GA parameters were kept to their default values. For each compound, a cluster analysis was then performed and the best scored conformation of the most populater cluster was kept as the binding conformation. ChemScore and GoldScore scoring functions were independently used to score interactions between ligand and target. Upon application of consensus scoring, a visual inspection of remaining entries led to ten selected compounds that were submitted to biological assays. As a result, the triazine derivative **15a** showed a submicromolar IC_{50} value (0.4 μM).

SciFinder Scholar was then applied to search for commercially available derivatives of both **4a** and **15a**. Resulting compounds were docked into the DDX3 binding site and best ranked entries were purchased from Asinex and ChemBridge.[14]

Details of high-throughput docking (HTD)

The pharmacophoric model used to identify **4a** could suffer from intrinsic limitations affecting all the structure-based pharmacophoric models. In fact, it was built on the basis of the interactions between the natural ligand AMP and its binding site within the structure of DDX3 that were codified by the software LigandScout into pharmacophoric features. The application of such a model as a three-dimensional filter to screen in silico databases of compounds results, by definition, in the identification of compounds able to satisfy the geometrical constraints imposed by the pharmacophoric features of the model. As a consequence, compounds able to partially fit the model will be ranked with a low fit score and, probably, discarded. However, although these compounds are unable to fully mimic the interactions involving AMP, they could be in principle able to occupy the AMP binding site by means of interactions involving amino acid residues not interacting with AMP itself. On the basis of these considerations, with the purpose of finding compounds able to be accommodated within the AMP binding site of DDX3 and thus to potentially interfere with its enzymatic activity, a high-throughput docking approach (HTD) was also applied to the Asinex Gold collection. The computational protocol was based on a preliminary database optimization consisting in the application of a filter based on the rule of five that allowed to prune ~20% entries. Moreover, a rule-based approach was also applied to enumerate all the possible tautomers and protonation forms of each compound that were in turn individually docked by means of GOLD software toward the binding site of DDX3. Compounds classified as best scored by a consensus scoring approach based on both GoldScore and ChemScore scoring functions were selected to be further analysed. Visual inspection, chemical diversity, and commercial availability of the best ranked entries led us to choose ten compounds to be purchased and submitted directly to biological assays. Among them, a hit compound belonging to the class of triazine derivatives (**15a**), endowed with submicromolar activity (0.4 μM, Table 2), was identified. Compounds' binding poses resulting from docking simulations were also supported by GRID calculations performed to search minimum interaction points between several chemical probes and the ADP binding pocket on DDX3. GRID software was also applied with the aim of taking into consideration, at least in part, DDX3 flexibility by setting to 1 the Directive MOVE of the program. In fact, when MOVE = 1, flexible side chains tend to move toward the probes to facilitate hydrogen bond and electrostatic interactions. This setting was suggested by the presence of several flexible amino acids within the DDX3 AMP binding site, such as Arg 202, Lys 230, and Lys 288.

Chemistry

General: All commercially available chemicals were used as purchased (From Aldrich-Italia, Milan). CH_3CN was dried over CaH_2, *t*BuOH was dried over Mg/I_2, CH_2Cl_2 was dried over NaH, and THF and dioxane were dried over Na/benzophenone prior to use, while DMF was bought already anhydrous. Anhydrous reactions were run under a positive pressure of dry N_2 or argon. IR spectra were

recorded on a PerkinElmer BX FTIR system, using KBr pellets. TLC was carried out using Merck TLC plates silica gel 60 F254. Chromatographic purifications were performed on columns packed with Merk 60 silica gel, 23–400 mesh, for flash technique. ^{1}H NMR and ^{13}C NMR spectra were recorded at 400 MHz on a Brucker Avance DPX400, at 300 MHz on a Varian VXR-300, and at 200 MHz on a Bruker AC200F spectrometer. Chemical shifts are reported relative to $(CH_3)_4Si$ at 0.00 ppm. Elemental analyses (C, H, N) were performed in-house using a PerkinElmer 240C Elemental Analyzer, and the data for C, H, and N are within 0.4% of the theoretical values. Melting points were taken using a Gallenkamp melting point apparatus and are uncorrected. MS data were obtained using an Agilent 1100 LC/MSD VL system (G1946C) with a 0.4 mL min^{-1} flow rate using a binary solvent system of MeOH/H_2O (95:5). UV detection was monitored at 254 nm. MS were acquired in positive and negative mode scanning over the mass range 50–1500. The following ion source parameters were used: drying gas flow, 9 mL min^{-1}; nebulizer pressure, 40 psig; drying gas temperature, 350 °C. All target compounds possessed a purity of $\geq$95% as verified by elemental analyses by comparison with the theoretical values.

Microwave irradiation experiments were conducted using a CEM Discover Synthesis Unit (CEM Corp., Matthews, NC, USA). The apparatus consists of a continuous focused microwave power delivery system with operator-selectable power output from 0 to 300 W. The temperature of the contents of the vessels was monitored using a calibrated IR temperature control mounted under the reaction vessel. All experiments were performed using a stirring option whereby the contents of the vessel are stirred by means of a rotating magnetic plate located below the floor of the microwave cavity and a Teflon-coated magnetic stir bar in the vessel.

3-(4-Oxo-2-thioxothiazolidin-3-yl)propanoic acid (2): To a solution of β-alanine **1** (3.4 g, 38.1 mmol) in 17 mL of 22% KOH solution, CS_2 (2.5 mL, 42 mmol) was added dropwise in such a manner that the temperature of the reaction did not exceed 25 °C. The mixture was allowed to stir at room temperature (RT) for ~3 h and then bromoacetic acid (5.3 g, 38.1 mmol) was added portionwise over 20 min. The reaction mixture was stirred at RT for additional 3 h during which a precipitate formed. The pH of the reaction mixture was adjusted to 3–4 using conc. H_2SO_4, and the resulting solution was stirred overnight at RT. The precipitate was filtered off and washed with H_2O to afford the desired compound **2** as a yellow solid (3.52 g, 45%); mp: 155–156 °C; ^{1}H NMR (400 MHz, CD_3OD): δ = 5.00 (brs, 1H), 4.22 (t, J = 7.5, 2H), 4.11 (s, 1H), 2.64 ppm (t, J = 7.6, 2H); ^{13}C NMR (100 MHz, CH_3OD): δ = 202.6, 174.4, 172.9, 39.6, 35.1, 30.3 ppm; MS (ESI): m/z: 204.1 [M−H]$^-$; Anal. calcd for $C_6H_7NO_3S_2$: C 35.11, H 3.44, N 6.82, found: C 35.10, H 3.48, N 6.88.

***N*-(2-Hydroxyphenyl)-3-(4-oxo-2-thioxothiazolidin-3-yl)propanamide (3a)**: Compound **2** (1.0 g, 4.87 mmol) and *N*,*N*-diisopropylethylamine (932 μL, 5.36 mmol) were dissolved in 20 mL of dry 1,2-dichloroethane. Subsequently, pivaloyl chloride (660 μL, 5.36 mmol) was added dropwise. The reaction mixture was stirred at RT for 3 h and then 2-aminophenol (531 mg, 4.87 mmol) was added. The mixture was allowed to stir at RT for additional 18 h. The solvent was removed under reduced pressure and the mixture was purified by flash chromatography using a mixture of hexane/EtOAc (1:1) to give the desired product **3a** as a yellow solid (1.23 g, 85%); mp: 168–170 °C; ^{1}H NMR (400 MHz, [D$_6$]DMSO): δ = 9.65 (s, 1H), 9.36 (s, 1H), 7.63 (d, J = 7.7 1H), 6.95–6.91 (m, 1H) 6.83 (d, J = 7.8, 1H) 6.75–6.72 (m, 1H), 4.24 (s, 2H), 4.13 (t, J = 7.4, 2H), 2.68 ppm (t, J = 7.5, 2H); ^{13}C NMR (50 MHz, [D$_6$]DMSO): δ = 202.8, 174.0, 168.5, 148.1, 125.8, 124.7, 122.9, 118.8, 115.6, 38.2, 35.7, 32.6 ppm; MS (ESI) m/z: 295.4 [M−H]$^-$; Anal. calcd for $C_6H_7NO_3S_2$: C 35.11, H 3.44, N 6.82, found: C 35.10, H 3.48, N 6.88.

***N*-(2-Nitrophenyl)-3-(4-oxo-2-thioxothiazolidin-3-yl)propanamide (3b)**: To a suspension of **2** (100 mg, 0.48 mmol) in 4 mL of dry CH_2Cl_2, thionyl chloride (40 μL, 0.58 mmol) was added. The reaction was monitored by TLC and after the disappearance of the starting material, 2-nitroaniline (80 mg, 0.58 mmol) was added. The resulting mixture was stirred at RT for 2 h. Subsequently, H_2O was added to the reaction mixture. The organic phase was separated and the aqueous phase was extracted with EtOAc. The combined organic phases were then dried over Na_2SO_4, concentrated under reduced pressure, and purified by flash chromatography using a mixture of hexane/EtOAc (1:1) to give the desired product **3b** as a yellow solid (130 mg, 84%); mp: 170–171 °C; ^{1}H NMR (400 MHz, $CDCl_3$): δ = 10.27 (s, 1H), 8.64–8.62 (m, 1H), 8.15–8.13 (m, 1H), 7.60–7.56 (m, 1H), 7.15–7.11 (m, 1H), 4.45 (t, J = 8, 2H), 3.94 (s, 2H), 2.22 ppm (t, J = 8, 2H); ^{13}C NMR (100 MHz, [D$_6$]DMSO): δ = 206.2, 174.0, 168.8, 136.0, 134.2, 128.0, 125.8, 123.6, 122.4, 40.3, 35.4, 34.9 ppm; MS (ESI) m/z: 324.4 [M−H]$^-$; Anal. calcd for $C_{12}H_{11}N_3O_4S_2$: C 44.30, H 3.41, N 12.91, found: C 44.36, H 3.38, N 12.90.

General procedure for the synthesis of 4a–h (Method A). To a solution of intermediate **3a** or **3b** (0.33 mmol) in 4 mL of EtOH, the appropriate benzaldehyde (0.33 mmol) and Et_3N (0.33 mmol) were added. The reaction mixture was held at reflux for 1 h, and the formed precipitate was filtered off and washed with EtOH and hexane to give the desired pure product.

General procedure for microwave-assisted synthesis of 4a–h (Method B). A mixture of intermediate **3a** or **3b** (0.16 mmol) and the appropriate benzaldehyde (0.16 mmol) was microwave irradiated for 5 min at 130 °C (3 cycles). The resulting residue was washed with EtOH and hexane to give the desired pure compound.

3-[(*Z*)-5-(3-Bromobenzylidene)-4-oxo-2-thioxothiazolidin-3-yl]-*N*-(2-hydroxyphenyl)propanamide (4a): Yellow solid; mp: 222–224 °C; ^{1}H NMR (400 MHz, [D$_6$]DMSO): δ = 9.56 (s, 1H), 9.38 (s, 1H), 7.89 (s, 1H), 7.81 (s, 1H), 7.71 (d, J = 7.9 1H), 7.65–7.60 (m, 2H), 7.53–7.49 (m, 1H), 6.92–6.90 (m, 1H) 6.83 (d, J = 7.8, 1H) 6.75–6.72 (m, 1H), 4.32 (t, J = 7.1, 2H), 2.79 ppm (t, J = 7.1, 2H); ^{13}C NMR (100 MHz, [D$_6$]DMSO): δ = 193.4, 169.1, 167.1, 148.7, 135.9, 133.9, 133.9, 132.0, 131.5, 129.0, 126.4, 125.3, 124.7, 123.4, 123.1, 119.3, 116.1, 41.4, 33.4 ppm; MS (ESI): m/z: 462.9 [M−H]$^+$; Anal. calcd for $C_{19}H_{15}BrN_2O_3S_2$: C 49.25, H 3.26, N 6.05, found: C 49.31, H 3.29, N 6.06.

3-[(*Z*)-5-(3-Fluorobenzylidene)-4-oxo-2-thioxothiazolidin-3-yl]-*N*-(2-hydroxyphenyl)propanamide (4b): Yellow solid (45%); mp: 210–211 °C; ^{1}H NMR (400 MHz, [D$_6$]acetone): δ = 9.17 (s, 1H), 7.69 (s, 1H), 7.59–7.54 (m, 1H), 7.44–7.41 (m, 1H), 7.37 (d, J = 8, 1H), 7.26–7.21 (m, 1H), 6.97–6.92 (m, 1H), 6.82 (d, J = 8 1H), 6.76–6.72 (m, 1H), 4.45 (t, J = 7.1, 2H), 2.92 ppm (t, J = 7.1, 2H); ^{13}C NMR (75 MHz, [D$_6$]DMSO): δ = 193.7, 169.3, 167.4, 164.7, 161.4, 148.9, 136.1, 135.9, 132.4, 132.2, 132.0, 126.8, 126.7, 126.6, 126.5, 124.9, 123.6, 119.6, 118.5, 118.2, 118.2, 117.9, 116.3, 40.9, 33.3 ppm. MS (ESI): m/z: 401.5 [M−H]$^-$; Anal. calcd for $C_{19}H_{15}FN_2O_3S_2$: C 56.70, H 3.76, N 6.96, found: C 56.76, H 3.75, N 6.98.

3-[(*Z*)-5-(3,5-Difluorobenzylidene)-4-oxo-2-thioxothiazolidin-3-yl]-*N*-(2-hydroxyphenyl)propanamide (4c): Yellow solid (77%); mp: 235–237 °C; ^{1}H NMR (400 MHz, [D$_6$]DMSO): δ = 9.56 (s, 1H), 9.30 (s, 1H), 7.72 (s, 1H), 7.58–7.56 (m, 1H), 7.37–7.33 (m, 1H), 7.28–7.27 (m, 2H), 6.87–6.83 (m, 1H), 6.77–6.75 (m, 1H), 6.68–6.64 (m, 1H), 4.23 (t, J = 7.16, 2H), 2.70 ppm (t, J = 7.16, 2H); ^{13}C NMR (100 MHz, [D$_6$]DMSO): δ = 193.1, 169.0, 167.0, 164.4, 164.2, 161.9, 161.8, 148.6, 136.7, 130.3, 126.3, 126.1, 125.2, 123.3, 119.3, 116.0,

113.7, 113.4, 106.8, 106.5, 106.3, 41.4, 33.3 ppm. MS (ESI): *m/z*: 419.4 $[M-H]^-$; Anal. calcd for $C_{19}H_{14}F_2N_2O_3S_2$: C 54.28, H 3.36, N 6.66, found: C 54.30, H 3.30, N 6.68.

3-[(*Z*)-5-(3-Methylbenzylidene)-4-oxo-2-thioxothiazolidin-3-yl]-*N*-(2-hydroxyphenyl)propanamide (4d): Yellow solid (61%); mp: 208–209 °C; ^{1}H NMR (400 MHz, [D$_6$]DMSO): $\delta=9.57$ (s, 1H), 9.30 (s, 1H), 7.69 (s, 1H), 7.57 (d, $J=8$, 1H), 7.39–7.36 (m, 3H), 7.27–7.25 (m, 1H), 6.87–6.83 (m, 1H), 6.76 (d, $J=8$, 1H), 6.69–6.64 (m, 1H), 4.25 (t, $J=7.2$, 2H), 2.72 ppm (t, $J=7.2$, 2H); ^{13}C NMR (100 MHz, [D$_6$]DMSO): $\delta=193.7$, 169.0, 167.2, 148.6, 139.3, 133.4, 132.1, 131.4, 129.8, 128.2, 126.3, 125.2, 123.3, 122.6, 119.3, 116.1, 41.2, 33.3, 21.3 ppm; MS (ESI): *m/z*: 397.5 $[M-H]^-$; Anal. calcd for $C_{20}H_{18}N_2O_3S_2$: C 60.28, H 4.55, N 7.03, found: C 60.21, H 4.59, N 7.12.

3-[(*Z*)-5-(3-Methoxybenzylidene)-4-oxo-2-thioxothiazolidin-3-yl]-*N*-(2-hydroxyphenyl)propanamide (4e): Yellow solid (67%); mp: 200–202 °C; ^{1}H NMR (400 MHz, [D$_6$]DMSO): $\delta=9.31$ (s, 1H), 7.73 (s, 1H), 7.57 (d, $J=8$, 1H), 7.42–7.38 (m, 1H), 7.14–7.12 (m, 2H), 7.03–7.01 (m, 1H), 6.87–6.83 (m, 1H), 6.76 (d, $J=8$, 1H), 6.68–6.64 (m, 1H), 4.25 (t, $J=7.2$, 2H), 2.72 ppm (t, $J=7.2$, 2H); ^{13}C NMR (100 MHz, [D$_6$]DMSO): $\delta=193.7$, 169.1, 160.2, 148.7, 134.8, 133.3, 131.1, 126.4, 125.3, 123.4, 122.9, 119.3, 117.5, 116.3, 116.2, 55.8, 41.4, 33.4 ppm; MS (ESI): *m/z*: 413.5 $[M-H]^-$; Anal. calcd for $C_{20}H_{18}N_2O_4S_2$: C 57.95, H 4.38, N 6.76, found: C 57.97, H 4.44, N 6.70.

3-{(*Z*)-5-[(Benzo[*d*][1,3]dioxol-5-yl)methylene]-4-oxo-2-thioxothiazolidin-3-yl}-*N*-(2-hydroxyphenyl)propanamide (4f). Yellow solid (53%); mp: 240–241 °C; ^{1}H NMR (400 MHz, [D$_6$]DMSO): $\delta=9.56$ (s, 1H), 9.30 (s, 1H), 7.66 (s, 1H), 7.58–7.56 (m, 1H), 7.14–7–12 (m, 1H), 7.09 (s, 1H), 7.04–7.01 (m, 1H), 6.87–6.84 (m, 1H), 6.77–6.75 (m, 1H), 6.68–6.65 (m, 1H), 6.07 (s, 2H), 4.23 (t, $J=7.2$, 2H), 2.70 ppm (t, $J=7.2$, 2H); ^{13}C NMR (100 MHz, [D$_6$]DMSO): $\delta=193.3$, 169.0, 167.2, 150.3, 148.8, 148.6, 133.5, 127.6, 127.4, 126.3, 125.2, 123.3, 120.2, 119.3, 116.1, 110.0, 109.7, 102.6, 41.2, 33.3 ppm. MS (ESI): *m/z*: 427.0 $[M-H]^-$; Anal. calcd for $C_{20}H_{16}N_2O_5S_2$: C 56.06, H 3.76, N 6.54, found: C 56.03, H 3.84, N 6.51.

3-[(*Z*)-5-(3-Bromobenzylidene)-4-oxo-2-thioxothiazolidin-3-yl]-*N*-(2-nitrophenyl)propanamide (4g): Yellow solid (85%); mp: 204–206 °C; ^{1}H NMR (400 MHz, [D$_6$]DMSO): $\delta=10.32$ (s, 1H), 7.87–7.84 (m, 1H), 7.79 (s, 1H), 7.72 (s, 1H), 7.63–7.60 (m, 2H), 7.54–7.52 (m, 2H), 7.45–7.41 (m, 1H), 7.31–7.27 (m, 1H), 4.23 (t, $J=7.4$, 2H), 2.70 ppm (t, $J=7.4$, 2H); ^{13}C NMR (100 MHz, [D$_6$]DMSO): $\delta=193.4$, 168.9, 167.0, 143.0, 135.8, 134.3, 133.8, 131.9, 131.4, 131.2, 129.0, 126.0, 125.8, 125.2, 124.7, 123.0, 40.9, 33.2 ppm. MS (ESI): *m/z*: 491.4 $[M-H]^-$; Anal. calcd for $C_{19}H_{14}BrN_3O_4S_2$: C 46.35, H 2.87, N 8.53, found: C 46.42, H 2.85, N 8.56.

3-[(*Z*)-5-(3-Fluorobenzylidene)-4-oxo-2-thioxothiazolidin-3-yl]-*N*-(2-nitrophenyl)propanamide (4h): Yellow solid (77%); mp: 207–208 °C; ^{1}H NMR (400 MHz, [D$_6$]DMSO): $\delta=10.32$ (s, 1H), 7.87–7.85 (m, 1H), 7.74 (s, 1H), 7.64–7.60 (m, 1H), 7.54–7.52 (m, 2H), 7.45–7.42 (m, 1H), 7.39–7.37 (m, 1H), 7.31–7.27 (m, 2H), 4.23 (t, $J=8$, 2H), 2.70 ppm (t, $J=8$, 2H); ^{13}C NMR (100 MHz, [D$_6$]DMSO): $\delta=$ 193.6, 169.0, 167.1, 164.0, 161.6, 143.1, 135.8, 135.7, 134.4, 132.1, 132.0, 131.8, 131.3, 126.5, 126.1, 125.9, 125.3, 124.7, 118.3, 118.1, 117.9, 117.7, 40.9, 33.3 ppm. MS (ESI): *m/z*: 430.5 $[M-H]^-$; Anal. calcd for $C_{19}H_{14}FN_3O_4S_2$: C 52.89, H 3.27, N 9.74, found: C 52.80, H 3.26, N 9.81.

General procedure for the synthesis of the inverted amide derivatives 7a,b: To a solution of bis(carboxymethyl)trithiocarbonate **5** (1 equiv) in dimethoxyethane (2 mL), Et_3N (1 equiv) and amine **6** (1 equiv, synthesized following a reported procedure)[17] were added. The reaction mixture was heated at 90 °C under microwave irradiation for 10 min. Then the appropriate aldehyde (1 equiv) was added and the mixture was heated at 110 °C under microwave irradiation for 5 min. The reaction mixture was evaporated to dryness. MeOH was added to the residue and a precipitate was formed upon standing. The solid was isolated by filtration, washed with hexane, and dried under high vacuum to give the final compounds **7a**,**b**.

***N*-{2-{(*Z*)-5-(3-Bromobenzylidene)-4-oxo-2-thioxothiazolidin-3-yl]ethyl}-2-hydroxybenzamide (7a)**: Yellow solid (69%); ^{1}H NMR (400 MHz, [D$_6$]DMSO): $\delta=12.32$ (s, 1H), 8.86 (t, $J=5.2$ Hz, 1H), 7.80 (s, 1H), 7.71 (s, 1H), 7.63 (d, $J=7.9$ Hz, 1H), 7.57–7.54 (m, 2H), 7.44 (t, $J=7.9$ Hz, 1H), 7.30 (t, $J=7.7$ Hz, 1H), 6.78 (t, $J=8.6$ Hz, 2H), 4.20 (t, $J=5.2$ Hz, 1H), 3.57 ppm (q, $J=5.2$ Hz, 1H); ^{13}C NMR (100 MHz, [D$_6$]DMSO): $\delta=194.2$, 170.2, 167.6, 160.7, 135.9, 133.9, 131.1, 129.0, 128.1, 124.8, 123.1, 115.4, 44.4, 36.7 ppm; MS (ESI) *m/z*: 462.9 $[M-H]^-$; Anal. calcd for $C_{19}H_{15}BrN_2O_3S_2$: C 49.25, H 3.26, N 6.05, found: C 49.19, H 3.34, N 6.12.

***N*-{2-[(*Z*)-5-(3-Fluorobenzylidene)-4-oxo-2-thioxothiazolidin-3-yl]ethyl}-2-hydroxybenzamide (7b)**: Yellow solid (62%); ^{1}H NMR (400 MHz, [D$_6$]DMSO): $\delta=12.31$ (1H, s), 8.85 (t, $J=4.6$ Hz, 1H), 7.72 (1H, s), 7.58–7.50 (m, 2H), 7.45–7.37 (m, 2H), 7.31–7.29 (m, 2H), 6.80–6.76 (m, 2H), 4.20 (t, $J=4.5$ Hz, 2H), 3.56 ppm (q, $J=4.6$ Hz, 2H); ^{13}C NMR (100 MHz, [D$_6$]DMSO): $\delta=193.8$, 169.8, 167.2, 164.8, 160.2, 135.4, 133.7, 131.7, 131.6, 130.8, 127.6, 126.0, 125.9, 124.3, 118.6, 117.4, 114.9, 43.9, 36.2 ppm; MS (ESI): *m/z*: 401.5 $[M-H]^-$; Anal. calcd for $C_{19}H_{15}FN_2O_3S_2$: C 56.70, H 3.76, N 6.96, found: C 56.59, H 3.83, N 6.84.

(*E*)-3-(3-bromobenzylidene)dihydrofuran-2,5-dione (9): To a solution of *t*BuOK, from 1.13 g (29 mmol, 1.2 equiv) of potassium in 15 mL of *tert*-butyl alcohol, 4.86 mL of diethyl succinate (29 mmol, 1.2 equiv) in 2.8 mL of *tert*-butyl alcohol were added dropwise. A solution of 3-bromobenzaldehyde **8** (2.82 mL, 1 equiv) in 2.6 mL of tert-butyl alcohol was added dropwise, and the resulting heterogeneous mixture was held at reflux for 2 h and then stirred at RT overnight. After cooling, 30 mL of H_2O were added and *tert*-butyl alcohol was removed by distillation. To this mixture, a solution of 3.12 g (55.6 mmol, 2.3 equiv) of KOH in 10 mL of H_2O was added. After holding at reflux for 4 h, the mixture was washed with Et_2O. The aqueous layer was treated with conc. HCl until pH 1 was reached. The solution was stirred for 5 min and then it was extracted with EtOAc. The organic phase was dried over Na_2SO_4 and finally evaporated under reduced pressure. The crude material was recrystallized from cyclohexane/hexane. The latter intermediate (1.67 g, 5.86 mmol, 1 equiv) was dissolved in THF, then acetic anhydride (1.22 mL, 2.2 equiv) was added and the resulting mixture stirred at RT for 5 h. Next THF was removed and methyl *tert*-butyl ether (MTBE) was added to induce a more complete crystallization. The crystals were filtered, washed with MTBE and dried in vacuo to yield the desired compound **9** as a white solid (2.26 g, 35%); mp: 151–152 °C; ^{1}H NMR (400 MHz, [D$_6$]DMSO): $\delta=7.80$ (s, 1H), 7.62–7.53 (m, 3H), 3.94–3.95 ppm (m, 2H); MS (ESI) *m/z*: 266 $[M-H]^-$; Anal. calcd for $C_{11}H_7BrO_3$: C 49.47, H 2.64, found: C 49.56, H 2.66.

3-[(*E*)-3-(3-bromobenzylidene)-2,5-dioxopyrrolidin-1-yl]propanoic acid (10): Compound **9** (0.564 mmol) and β-alanine (150 mg, 0.564 mmol) were dissolved in dry DMF and the solution was heated under microwave irradiation (200W) at 150 °C for 10 min. H_2O was added and the resulting mixture was extracted with CH_2Cl_2. The organic phases were collected, washed with brine, and dried over Na_2SO_4. The solvent was removed under reduced pres-

sure, and the residue was crystallized in EtOH to obtain the desired product **10** as a white solid (78 mg, 42%). ^{1}H NMR (400 MHz, [D$_6$]DMSO): δ = 12.31 (brs, 1H), 7.76 (s, 1H), 7.62–7.52 (m, 2H), 7.39–7.31 (m, 2H), 3.66 (t, J = 7.5, 2H,), 2.47 ppm (t, J = 7.5 Hz, 2H); MS (ESI): m/z: 337.1 [M−H]$^-$; Anal. calcd for $C_{14}H_{12}BrNO_4$: C 49.73, H 3.58, N 4.14, found: C 49.70, H 3.63, N 4.08.

3-[(*E*)-3-(3-bromobenzylidene)-2,5-dioxopyrrolidin-1-yl]-*N*-(2-hydroxyphenyl)propanamide (11): Compounds **10** (72 mg, 0.259 mmol, 1 equiv) and DIPEA (50 μL, 0.285 mmol, 1.1 equiv) were dissolved in DCE (3 mL). Subsequently, pivaloyl chloride (35 μL, 0.285 mmol, 1.1 equiv) was added dropwise and the resulting mixture was stirred at RT for 1 h. Then aminophenol (27 mg, 0.247 mmol, 0.95 equiv) was added and the mixture was stirred at RT overnight. The solvent was removed and the resulting residue was crystallized in EtOH to obtain the final product **11** as a white solid (72 mg, 62%); mp: 226–228 °C; ^{1}H NMR (400 MHz, [D$_6$]DMSO): δ = 9.54 (s, 1H), 9.28 (s, 1H), 7.77 (s, 1H), 7.60–7.53 (m, 3H), 7.41–7.31 (m, 2H), 6.86 (t, J = 7.4 Hz, 1H), 6.76 (d, J = 7.6 Hz, 1H), 6.67 (t, J = 7.4 Hz, 1H), 3.71 (t, J = 7.1 Hz, 2H), 3.66 (s, 2H), 2.61 ppm (t, J = 7.1 Hz, 2H); ^{13}C NMR (100 MHz, [D$_6$]DMSO): δ = 173.8, 170.1, 168.2, 148.2, 136.4, 132.5, 132.3, 130.9, 130.3, 128.7, 126.9, 125.3, 124.6, 123.9, 122.2, 118.8, 115.7, 34.8, 33.6, 33.5 ppm; MS (ESI): m/z: 428.3 [M−H]$^-$; Anal. calcd for $C_{20}H_{17}BrN_2O_4$: C 55.96, H 3.99, N 6.53, found: C 55.88, H 4.06, N 6.46.

General procedure for the synthesis of compounds 13a–c: To a stirred solution of cyanuric chloride **12** (1 g, 5.42 mmol) in dimethoxyethane (35 mL) at −30 °C, the appropriate benzylamine (1 equiv) was added dropwise. The reaction mixture was vigorously stirred for 3 h at −30 °C, then warmed to RT and washed successively with 3N HCl, H_2O, and brine. The organic phase was dried over anhydrous Na_2SO_4 and then evaporated to dryness. The resulting white residue was dissolved in a minimum amount of CH_2Cl_2. Finally, by addition of petroleum ether, the final compound was precipitated and collected by filtration.

***N*-Benzyl-4,6-dichloro-1,3,5-triazin-2-amine (13a)**: Yield 85%; ^{1}H NMR (200 MHz, $CDCl_3$): δ = 7.30–7.26 (m, 5H), 4.48 ppm (m, 2H); MS (ESI): m/z: 256.1 [M+H]$^+$; Anal. calcd for $C_{10}H_9Cl_2N_4$: C 47.08, H 3.16, N 21.96, found: C 47.02, H 3.21, N 22.04.

4,6-Dichloro-*N*-(4-fluorobenzyl)-1,3,5-triazin-2-amine (13b): Yield 75%; mp: 151.0–151.5 °C; ^{1}H NMR (400 MHz, CD_3OD): δ = 7.23–7.19 (m, 2H), 6.98 (t, J = 8.48 Hz, 2H), 6.19 (brs,1H); MS (ESI) m/z: 274.1 [M+H]$^+$; Anal. calcd for $C_{10}H_7Cl_2FN_4$: C 43.98, H 2.58, N 20.52, found: C 43.88, H 2.62, N 20.59.

4,6-Dichloro-*N*-(3-chlorobenzyl)-1,3,5-triazin-2-amine (13c): Yield 78%; mp: 149 °C; ^{1}H NMR (400 MHz, CD_3OD): δ = 7.23–7.19 (m, 3H), 7.13–7.10 (m, 1H), 6.58 (brs, 1H), 4.60 ppm (d, J = 6.29 Hz, 2H); ^{13}C NMR (100 MHz, $CDCl_3$): δ = 170.0, 166.0, 138.5, 134.8, 130.2, 128.2, 127.7, 125.7, 44.7 ppm. MS (ESI): m/z: 289.5 [M+H]$^+$; 311.5 [M+Na]$^+$; Anal. calcd for $C_{10}H_7Cl_3N_4$: C 41.48, H 2.44, N 19.35, found: C 41.45, H 2.38, N 19.36.

General procedure for the synthesis of compounds 14a–d: To a suspension of the appropriate intermediate **13a–c** (1 equiv) in CH_2Cl_2, the appropriate amine (2 equiv) was added dropwise. The reaction mixture was stirred at RT for 12 h and then washed successively with 3N HCl, H_2O, and brine. The organic phase was dried over anhydrous Na_2SO_4 and evaporated to dryness. The resulting white residue was dissolved in a minimum amount of CH_2Cl_2. Finally, by addition of petroleum ether, the final compound precipitated and was collected by filtration.

***N*-Benzyl-4-chloro-6-morpholino-1,3,5-triazin-2-amine (14a)**: Yield 67%; ^{1}H NMR (200 MHz, $CDCl_3$): δ = 7.28–7.25 (m, 5H), 7.07 (brs, 1H), 4.58 (d, J = 6 Hz, 2H), 3.74–3.65 ppm (m, 8H). MS (ESI): m/z: 306.8 [M+H]$^+$; Anal. calcd for $C_{14}H_{16}ClN_5O$: C 54.99, H 5.27, N 22.90, found: C 55.05, H 5.25, N 22.87.

***N*2-Benzyl-6-chloro-*N*4,*N*4-diethyl-1,3,5-triazine-2,4-diamine (14b)**: Yield 75%; ^{1}H NMR (200 MHz, $CDCl_3$): δ = 7.29–7.24 (m, 5H), 6.06 (brs, 1H), 4.57 (s, 2H), 3.55–3.48 (m, 4H), 1.16–1.07 (m, 6H); MS (ESI): m/z: 292.8 [M+H]$^+$; Anal. calcd for $C_{14}H_{15}Cl_2N_5$: C 57.63, H 6.22, N 24.00, found: C 57.60, H 6.16, N 24.08.

4-Chloro-*N*-(3-chlorobenzyl)-6-morpholino-1,3,5-triazin-2-amine (14c): Yield 85%; mp: 168–168.5 °C; ^{1}H NMR (400 MHz, CD_3OD): δ = 7.72 (s, 1H), 7.19–7.16 (m, 2H), 6.67 (brs, 1H), 4.54–4.49 (m, 2H), 3.72–3.61 ppm (m, 8H); ^{13}C NMR (100 MHz, $CDCl_3$): δ = 165.46, 164.34, 163.10, 144.97, 134.07, 129.34, 128.90, 128.82, 115.42, 115.21, 66.54, 66.37, 44.03, 43.79 ppm; MS (ESI): m/z: 340.1 [M+H]$^+$; Anal. calcd for $C_{14}H_{15}Cl_2N_5$: C 49.43, H 4.44, N 20.59, found: C 49.40, H 4.46, N 20.51.

4-Chloro-*N*-(4-fluorobenzyl)-6-morpholino-1,3,5-triazin-2-amine (14d): Yield 95%; mp: 192 °C; ^{1}H NMR (400 MHz, CD_3OD): δ = 7.23–7.17(m, 2H), 6.95 (t, J = 8.43, 2H), 6.00 (brs, 1H), 4.52–4.47 (m, 2H), 3.72 (s, 4H), 3.62 ppm (s, 4H); MS (ESI) m/z: 324.7 [M+H]$^+$. Anal. calcd for $C_{14}H_{15}ClFN_5O$: C 51.94, H 4.67, N 21.63, found: C 51.88, H 4.74, N 21.60.

General procedure for the synthesis of compounds 15e–g and 16i,j,o,p. To a solution of the appropriate intermediate **14a–d** (1 equiv) in CH_2Cl_2, hydrazine (4 equiv) was added and the resulting mixture was held at reflux for 12 h. After cooling down to RT, the mixture was washed with H_2O and brine. The organic phase was dried over anhydrous Na_2SO_4 and evaporated to dryness. The resulting residue was dissolved in toluene and reacted with the appropriate aldehyde (2 equiv). The reaction mixture was held at reflux for 3 h using a Dean–Stark apparatus for azeotropical removal of H_2O. The reaction mixture was evaporated to dryness and the resulting residue was dissolved in a minimum amount of CH_2Cl_2. Upon subsequent addition of petroleum ether, the desired compounds **15e–g** and **16i,j,o,p** precipitated and were collected by filtration.

(*E*)-2-({2-[4-(Benzylamino)-6-morpholino-1,3,5-triazin-2-yl]hydrazono}methyl)phenol (15e): Yield 80%; ^{1}H NMR (400 MHz, $CDCl_3$): δ = 12.39 (s, 1H), 8.87 (s, 1H), 7.60–7.58 (m, 1H), 7.34–7–30 (m, 6H), 6.96–6.95 (m, 1H), 6.83–6.81 (m, 1H), 6.15 (brs, 1H), 4.64 (s, 2H), 3.60–3.57 (m, 4H), 1.26–1.12 ppm (m, 6H); ^{13}C NMR ($CDCl_3$): δ = 164.4, 163.3, 141.2, 139.8, 138.2, 137.8, 129.9, 127.9, 126.8, 126.4, 122.2, 120.8, 120.2, 110.3, 44.0, 40.9, 12.0 ppm. MS (ESI): m/z: 431.5 [M+H]$^+$; Anal. calcd for $C_{22}H_{22}N_8O_2$: C 61.38, H 5.15, N 26.03, found: C 61.34, H 5.21, N 26.09.

(*Z*)-3-{2-[4-(3-Chlorobenzylamino)-6-morpholino-1,3,5-triazin-2-yl]hydrazono}indolin-2-one (15f): Yield 71%; mp: 144–144.5 °C; ^{1}H NMR (400 MHz, CD_3OD): δ = 12.39 (s, 1H), 8.15 (s, 1H), 7.62 (d, J = 6.80 Hz, 1H), 7.26 (s, 1H), 7.16 (m, 4H), 7.00–6.90 (m, 1H), 6.77 (d, J = 7.82 Hz), 4.53 (s, 2H), 3.75 (s, 4H), 3.65 (s, 4H); ^{13}C NMR (100 MHz, $CDCl_3$): δ = 165.1, 164.3, 163.1, 141.1, 139.8, 134.3, 132.4, 130.2, 129.8, 127.7, 127.3, 125.5, 122.9, 121.3, 120.9, 110.5, 66.8, 44.4, 43.8 ppm; MS (ESI) m/z: 465.9 [M+H]$^+$; Anal. calcd for $C_{22}H_{21}ClN_8O_2$: C 56.84, H 4.55, N 24.10, found: C 56.88, H 4.47, N 24.11.

(*E*)-3-{2-[4-(benzylamino)-6-(diethylamino)-1,3,5-triazin-2-yl]hydrazono}indolin-2-one (15g): Yield 78%; ^{1}H NMR (400 MHz, $CDCl_3$): δ = 11.52 (s, 1H), 7.92 (s, 2H), 7.33 (s, 3H), 7.18–7.17 (m,

1H), 7.01–6.99 (m, 1H), 6.91–6.87 (m, 1H), 4.63 (s, 2H), 3.82–3.73 (m, 8H); MS (ESI) *m/z*: 417.5 $[M+H]^+$; Anal. calcd for $C_{22}H_{24}N_8O$: C 63.45, H 5.81, N 26.90, found: C 63.53, H 5.88, N 26.81.

(*E*)-3-({2-[4-(Benzylamino)-6-morpholino]-1,3,5-triazin-2-yl}hydrazono)indolin-2-one (16j): Yield 74%; ^{1}H NMR (400 MHz, $CDCl_3$): $\delta = 12.47$ (s, 1H), 9.27 (s, 1H), 7.51–7.49 (m, 1H), 7.32–7.23 (m, 5H), 7.15–7.13 (m, 1H), 7.05–7.01 (m, 1H), 6.90–6.79 (m, 1H), 6.48 (brs, 1H), 4.64 (s, 2H), 3.84–3.72 ppm (m, 8H); ^{13}C NMR ($CDCl_3$): $\delta =$ 166.1, 165.1, 164.1, 163.3, 134.0, 138.8, 132.5, 123.0, 128.4, 127.4, 127.1, 122.7, 121.2, 120.7, 110.5, 66.7, 44.9, 43.7; MS (ESI): *m/z*: 406.5 $[M+H]^+$; Anal. calcd for $C_{21}H_{23}N_7O_2$: C 62.21, H 5.72, N 24.18, found: C 62.26, H 5.64, N 24.15.

(*E*)-2-({2-[4-(4-fluorobenzylamino)-6-morpholino-1,3,5-triazin-2-yl]hydrazono}methyl)phenol (16i). Yield 87%; mp: 114–114.5 °C. ^{1}H NMR (400 MHz, CD_3OD): $\delta = 11.48$ (s, 1H), 7.77 (s, 1H), 7.19 (s, 3H), 7.02 (s, 1H), 6.91 (s, 3H), 6.80 (t, $J = 6.63$ Hz, 1H), 4.47 (s, 2H), 3.74 (s, 4H), 3.65 ppm (s, 4H); ^{13}C NMR (100 MHz, $CDCl_3$): $\delta =$ 165.1, 163.9, 163.3, 160.8, 158.1, 143.9, 134.8, 130.8, 129.8, 129.2, 119.2, 118.2, 117.0, 115.5, 115.3, 66.8, 44.1, 43.7 ppm; MS (ESI): *m/z*: 424.4 $[M+H]^+$; 446.4 $[M+Na]^+$; Anal. calcd for $C_{21}H_{22}FN_7O_2$: C 59.57, H 5.24, N 23.15, found: C 59.56, H 5.06, N 23.14.

(*E*)-2-({2-[4-(3-chlorobenzylamino)-6-morpholino-1,3,5-triazin-2-yl]hydrazono}methyl)phenol (16o): Yield 82%; mp: 163.5–164 °C; ^{1}H NMR (400 MHz, CD_3OD): $\delta = 11.51$ (s, 1H), 7.83 (s, 1H), 7.29–7.07 (m, 3H), 6.96 (d, $J = 8.2$, 1H), 6.84 (t, $J = 7.4$, 3H), 4.54 (d, $J = 4.9$ Hz, 2H), 3.77 (s, 4H), 3.71 (s, 4H); ^{13}C NMR (100 Hz, $CDCl_3$): $\delta = 164.8$, 158.0, 143.9, 141.1, 134.3, 130.8, 129.8, 127.6, 127.3, 125.5, 119.1, 118.0, 116.9, 66.7, 44.2, 43.7; MS (ESI): *m/z*: 440.9 $[M+H]^+$; 462.9 $[M+Na]^+$; Anal. calcd for $C_{21}H_{22}ClN_7O_2$: C 57.34, H 5.04, N 22.29, found: C 57.37, H 5.12, N 22.21.

(*E*)-2-({2-[4-(benzylamino)-6-(diethylamino)-1,3,5-triazin-2-yl]hydrazono}methyl)phenol (16p). Yield 85%; ^{1}H NMR (400 MHz, $CDCl_3$): $\delta = 11.54$ (brs, 1H), 7.86 (s, 1H), 7.31–7.19 (m, 6H), 7.10–7.08 (m, 1H), 6.97–6.95 (m, 1H), 6.85–6.82 (m, 1H), 5.24 (brs, 1H), 4.59–4.57 (m, 2H), 3.56 (m, 4H), 1.18–1.11 ppm (m, 6H); MS (ESI) *m/z*: 392.5 $[M+H]^+$; Anal. calcd for $C_{21}H_{25}N_7O$: C 64.43, H 6.44, N 25.05, found: C 64.38, H 6.48, N 25.00.

4,6-Dichloro-*N*-(4-fluorophenyl)-1,3,5-triazin-2-amine (18): To a stirred solution of cyanuric chloride **12** (2 g, 10.86 mmol) in dimethoxyethane (20 mL) at −30 °C, 4-fluoroaniline (1 equiv) was added dropwise. The reaction mixture was vigorously stirred for 3 h at −30 °C, then warmed to RT, and washed with 3N HCl, H_2O, and brine. The organic phase was then dried over anhydrous Na_2SO_4 and evaporated to dryness. The obtained white residue was purified by flash chromatography using a mixture of petroleum ether/Et_2O (3:1) to give the desired product **18** and the side product **17**. Yield 35%; mp: 172 °C; ^{1}H NMR (400 MHz, $CDCl_3$): $\delta = 7.79$ (brs, 1H), 7.41 (q, $J = 8.60$ Hz, 2H), 7.03 ppm (t, $J = 8.63$ Hz, 2H); ^{13}C NMR (100 MHz, $CDCl_3$): $\delta = 171.3$, 164.3, 161.7, 159.2, 131.6, 123.8, 116.3 ppm; MS (ESI) *m/z*: 260.1 $[M+H]^+$; 282.1 $[M+Na]^+$; Anal. calcd for $C_9H_5Cl_2FN_4$: C 41.73, H 1.95, N 21.63, found: C 41.77, H 1.93, N 21.64.

6-Chloro-*N*2,*N*4-bis(4-fluorophenyl)-1,3,5-triazine-2,4-diamine (17): Yield 50%; ^{1}H NMR (400 MHz, $CDCl_3$): $\delta = 7.79$ (brs, 2H), 7.39–7.36 (m, 4H), 7.04–7.02 (m, 4H); MS (ESI): *m/z*: 334.7 $[M+H]^+$; Anal. calcd for $C_{15}H_{10}ClF_2N_5$: C 53.99, H 3.02, N 20.99, found: C 53.94, H 3.05, N 20.95.

4-Chloro-*N*-(4-fluorophenyl)-6-morpholino-1,3,5-triazin-2-amine (19). To a suspension of compound **18** (1 equiv) in CH_2Cl_2, morpholine (2 equiv) was added dropwise. The reaction mixture was stirred at RT for 12 h and then washed consecutively with 3N HCl, H_2O, and brine. The organic phase was then dried over anhydrous Na_2SO_4 and evaporated to dryness. The obtained white residue was dissolved in a minimum amount of CH_2Cl_2. Upon addition of petroleum ether, the final compound precipitated and was collected by filtration. Yield 82%; mp: 170–172 °C; ^{1}H NMR (400 MHz, $CDCl_3$): $\delta = 7.37$ (q, $J = 8.60$ Hz, 2H); 6.97 (t, $J = 8.63$ Hz, 2H); 3.78 (brs, 2H); 3.72 (brs, 2H); 3.67–3.66 ppm (m, 4H). MS (ESI): *m/z*: 310.7 $[M+H]^+$; 332.6 $[M+Na]^+$; Anal. calcd for $C_{13}H_{13}ClFN_5O$: C 50.41, H 4.23, N 22.61, found: C 50.44, H 4.28, N 22.58.

4-(4,6-Dichloro-1,3,5-triazin-2-yl)morpholine (22): To a stirred solution of cyanuric chloride **12** (1 g, 5.42 mmol) in dimethoxyethane (50 mL) at −30 °C, morpholine (470.1 μL, 5.42 mmol) was added dropwise. The reaction mixture was vigorously stirred for 3 h at −30 °C, then warmed to RT and washed consecutively with 3N HCl, H_2O, and brine. The organic phase was dried over anhydrous Na_2SO_4 and evaporated to dryness to yield the pure product **22** as a white solid. Yield 79%; mp: 156.7–156.9 °C; ^{1}H NMR (400 MHz, CD_3OD): $\delta = 3.80$ (t, $J = 4.59$ Hz, 4H); 3.66 ppm (t, $J = 4.59$ Hz, 4H); ^{13}C NMR (100 MHz, $CDCl_3$): $\delta = 170.4$, 164.1, 66.4, 44.5 ppm. MS (ESI): *m/z*: 235.1 $[M+H]^+$, 257.2 $[M+Na]^+$; Anal. calcd for $C_7H_8Cl_2N_4O$: C 35.77, H 3.43, N 23.83, found: C 35.74, H 3.38, N 23.92.

4-Chloro-*N*-(4-fluorophenyl)-6-morpholino-1,3,5-triazin-2-amine (23). To a stirred solution of compound **22** (650 mg, 2.76 mmol) in CH_2Cl_2, 4-fluoro aniline (310.81 μL, 2.71 mmol) was added. The reaction mixture was held at reflux for 12 h and then washed with 3N HCl, H_2O, brine and finally dried over anhydrous Na_2SO_4. The organic phase was evaporated to dryness and the white residue was dissolved in a minimum amount of CH_2Cl_2. Upon addition of petroleum ether the final compound precipitated as a white solid and was collected by filtration. Yield 90%. mp:170–172 °C; ^{1}H NMR (400 MHz, $CDCl_3$): $\delta = 7.38$ (q, $J = 8.60$ Hz, 2H); 6.97 (t, $J = 8.63$ Hz, 2H); 3.78 (brs, 2H); 3.72 (brs, 2H); 3.67–3.66 ppm (m, 4H) MS (ESI): *m/z*: 310.7 $[M+H]^+$; 332.6 $[M+Na]^+$; Anal. calcd for $C_{13}H_{13}ClFN_5O$: C 50.41, H 4.23, N 22.61, found: C 50.35, H 4.19, N 22.69.

General procedure for the synthesis of compounds 16m,n and 20b,c. To a solution of the appropriate intermediate **17**, **19**, or **23** (1 equiv) in CH_2Cl_2, hydrazine (4 equiv) was added and the resulting mixture was held at reflux for 12 h. After cooling to RT, the mixture was washed with H_2O and brine. The organic phase was dried over anhydrous Na_2SO_4 and evaporated to dryness. The obtained residue was dissolved in toluene and reacted with the appropriate aldehyde (2 equiv). The reaction mixture was held at reflux for 3 h using a Dean–Stark apparatus for azeotropical removal of H_2O and then evaporated to dryness. The resulting residue was dissolved in a minimum amount of CH_2Cl_2. Upon addition of petroleum ether the desired final compound precipitated and was collected by filtration.

Example: (*E*)-*N*-(4-Fluorophenyl)-4-morpholino-6-[2-(naphthalen-1-ylmethylene)hydrazinyl]-1,3,5-triazin-2-amine (20b): Yield 80%; mp: 220.0–220.4 °C; ^{1}H NMR (400 MHz, $CDCl_3$): $\delta = 8.62$ (m, 1H); 8.47 (m, 1H); 7.91–7.81 (m, 3H); 7.53–7.49 (m, 5H); 6.99 (t, $J =$ 8.4 Hz, 3H); 3.82 (s, 4H); 3.76 ppm (s, 4H); ^{13}C NMR (100 MHz, $CDCl_3$): $\delta = 165.9$, 161.1, 156.3, 142.6, 133.8, 128.8, 127.6, 127.0, 126.8, 126.3, 121.8, 115.1, 77.6, 77.0, 76.4, 66.8, 43.8 ppm; MS (ESI): *m/z*: 444.2 $[M+H]^+$; Anal. calcd for $C_{24}H_{22}FN_7O$: C 65.00, H 5.00, N 22.11, found: C 65.06, H 5.10, N 22.02.

(*E*)-*N*-(4-fluorophenyl)-4-morpholino-6-[2-(naphthalen-2-ylmethylene)hydrazinyl]-1,3,5-triazin-2-amine (20c): Yield 83%; mp: 225–226 °C; ^{1}H NMR (400 MHz, $CDCl_3$): $\delta = 10.95$ (brs, 1H), 8.22(s,1H),

7.93–7.83 (m, 6H), 7.46–7.44 (m,2H), 7.05 (t, $J=8.5$; 2H), 3.68 (s, 4H), 3.58 ppm (s, 4H); ^{13}C NMR (100, MHz, $CDCl_3$): $\delta=165.3$, 164.6, 158.9, 156.6, 142.9, 137.2, 133.8, 133.5, 133.4, 133.3, 128.8, 128.6, 128.2, 128.1, 127.1, 122.9, 121.8, 115.4, 115.2, 66.5, 43.9 ppm; MS (ESI): *m/z*: 444.5 $[M+H]^+$; Anal. calcd for $C_{24}H_{22}FN_7O$: C 65.00, H 5.00, N 22.11, found: C 65.05, H 5.09, N 22.14.

2-[6-(4-Fluorophenylamino)-2-(methylthio)pyrimidin-4-yl]ethanol (25): A mixture of **24** (0.28 mmol) and 4-fluoroaniline (1.12 mmol) in dimethoxyethane was microwave irradiated at 150 °C for 5 min. The reaction mixture was then concentrated under reduced pressure, diluted with EtOAc, and washed with H_2O. The organic phase was dried over anhydrous Na_2SO_4 and purified by flash chromatography using a mixture of CH_2Cl_2/EtOAc (1:1) to afford the desired product **25**. Yield 80%; ^{1}H NMR (400 MHz, $CDCl_3$): $\delta=7.3$ (m, 2H), 7.1 (t, 2H), 6.62 (s, 1H), 6.1 (s, 1H), 3.95 (t, $J=8$ Hz, 2H), 2.75 (t, $J=8$ Hz, 2H), 2.5 ppm (s, 3H); ^{13}C NMR (50 MHz, CD_3OD): $\delta=172.8$, 167.1, 162.7, 162.1, 157.9, 136.9, 123.8, 123.7, 116.4, 116.0, 101.8, 61.6, 41.0, 14.2 ppm. MS (ESI): *m/z*: 280.3 $[M+H]^+$; Anal. calcd for $C_{13}H_{14}FN_3OS$: C 55.90, H 5.05, N 15.04, found: C 55.95, H 5.12, N 15.08.

2-[6-(4-Fluorophenylamino)-2-(methylsulfonyl)pyrimidin-4-yl]ethanol (26): Compound **25** (0.448 mmol) was dissolved in a 1:1 mixture of MeOH and H_2O (6 mL). Then oxone (0.896 mmol) in 3 mL of H_2O was added portionwise, and the mixture was stirred overnight at RT. The crude mixture was concentrated under reduced pressure, neutralized with aq. $NaHCO_3$, and washed with EtOAc. The organic extracts were collected, dried over Na_2SO_4, and then evaporated under reduced pressure. The crude residue was purified by flash chromatography using a mixture of CH_2Cl_2/EtOAc (1:1) to give the desired product **26**. Yield 71%; ^{1}H NMR (200 MHz, $CDCl_3$): $\delta=7.55$ (br, 1H), 7.35 (m, 2H), 7.1 (m, 2H), 6.55 (s, 1H), 3.95 (t, $J=8$ Hz, 2H), 3.3 (s, 3H), 2.85 ppm (t, $J=8$ Hz, 3H); ^{13}C NMR (50 MHz, CD_3OD): $\delta=168.7$, 166.4, 163.2, 162.8, 158.8, 136.1, 124.1, 116.8, 116.3, 108.6, 61.1, 41.1, 39.3 ppm; MS (ESI): *m/z*: 312.3 $[M+H]^+$; Anal. calcd for $C_{13}H_{14}FN_3O_3S$: C 50.15, H 4.53, N 13.50, found: C 50.18, H 4.47, N 13.59.

6-[2-(*tert*-Butyldiphenylsilyloxy)ethyl]-*N*-(4-fluorophenyl)-2(methylsulfonyl)pyrimidin-4-amine (27): Compound **26** (0.16 mmol) and *tert*-butyldiphenylsilyl chloride (0.16 mmol) were dissolved in dry DMF and the mixture was microwave irradiated at 100 °C for 5 min. The reaction mixture was diluted with EtOAc, washed several times with H_2O and brine, and dried over Na_2SO_4. The crude material was purified by flash chromatography using a mixture of CH_2Cl_2/EtOAc (9:1) to give the desired product **27**. Yield 80%; ^{1}H NMR (200 MHz, $CDCl_3$): $\delta=7.55$ (m, 4H), 7.40 (m, 6H), 7.25 (m, 2H), 7.05 (m, 2H), 6.60 (s, 1H), 4.00 (t, $J=8$ Hz, 2H), 3.20 (s, 3H), 2.75 (t, $J=8$ Hz, 2H), 0.95 ppm (s, 9H); ^{13}C NMR (50 MHz, $CDCl_3$): $\delta=169.0$, 165.2, 163.1, 162.2, 158.1, 135.4, 133.2, 129.7, 127.7, 125.6, 125.5, 116.8, 116.3, 105.2, 62.0, 40.7, 38.8, 29.6, 26.7 ppm; MS (ESI): *m/z*: 550.7 $[M+H]^+$; Anal. calcd for $C_{29}H_{32}FN_3O_3SSi$: C 63.36, H 5.87, N 7.64, found: C 63.43, H 5.80, N 7.60.

6-[2-(*tert*-Butyldiphenylsilyloxy)ethyl]-*N*-(4-fluorophenyl)-2-hydrazinylpyrimidin-4-amine (28): Compound **27** (0.2 mmol) was dissolved in dimethoxyethane (2 mL) and the resulting mixture was microwave irradiated at 120 °C for 5 min. The solvent was evaporated under reduced pressure and the remaining crude material was purified by flash chromatography using a mixture of CH_2Cl_2/MeOH (19:1) to give the desired product **28**. Yield 90%; ^{1}H NMR (400 MHz, $CDCl_3$): $\delta=7.50$ (d, $J=4$ Hz, 4H), 7.27 (m, 6H), 7.2 (m, 2H), 6.95 (t, $J=8$ Hz, 2H), 5.87 (s, 1H); 3.89 (t, $J=8$ Hz, 2H), 2.61 (t, $J=8$ Hz, 2H), 0.91 ppm (s, 9H); ^{13}C NMR (100 MHz, $CDCl_3$): $\delta=162.0$, 161.0, 158.6, 135.4, 134.8, 134.5, 133.7, 129.6, 127.8, 127.6, 127.5, 124.8, 124.7, 116.1, 115.9, 95.3, 62.5, 40.8, 29.7, 26.8 ppm; MS (ESI): *m/z*: 502.7 $[M+H]^+$; Anal. calcd for $C_{28}H_{32}FN_5OSi$: C 67.04, H 6.43, N 13.96, found: C 67.12, H 6.40, N 13.94.

2-[(2-{4-[2-(*tert*-Butyldiphenylsilyloxy)ethyl]-6-(4-fluorophenylamino)pyrimidin-2-yl}hydrazono)methyl]phenol (29): Compound **28** (0.046 mmol) and salicylaldehyde (0.046 mmol) were dissolved in dry toluene containing molecular sieves. The mixture was held at reflux for 2 h, then cooled to RT, concentrated under reduced pressure, and purified by flash chromatography using a mixture of CH_2Cl_2/EtOAc (9:1) to give the desired product **29**. Yield 54%; ^{1}H NMR (200 MHz, $CDCl_3$): $\delta=8.05$ (s, 1H), 7.55 (d, $J=4$ Hz, 4H), 6.7–7.4 (m, 14H), 5.9 (s, 1H), 3.9 (t, $J=8$ Hz, 2H), 2.7 (t, $J=8$ Hz, 2H), 0.95 ppm (s, 9H); ^{13}C NMR (50 MHz, $CDCl_3$): $\delta=166.8$, 162.4, 162.2, 158.3, 158.0, 143.8, 135.5, 133.9, 133.9, 133.5, 130.5, 129.8, 129.6, 127.6, 124.6, 124.5, 119.1, 118.4, 116.9, 116.4, 116.0, 95.6, 62.2, 39.9, 29.6, 26.8 ppm; MS (ESI): *m/z*: 606.8 $[M+H]^+$; Anal. calcd for $C_{35}H_{36}FN_5O_2Si$: C 69.39, H 5.99, N 11.56, found: C 69.38, H 6.05, N 11.50.

2-({2-[4-(4-Fluorophenylamino)-6-(2-hydroxyethyl)pyrimidin-2-yl]hydrazono}methyl)phenol (30): Compound **29** (0.025 mmol) was dissolved in dry THF (2 mL). Then $Et_3N{\cdot}3HF$ (24 μL, 0.150 mmol) was added, and the resulting mixture was stirred overnight at RT. After addition of aq. $NaHCO_3$ to the reaction mixture, it was extracted with EtOAc, dried over Na_2SO_4, and evaporated. The crude material was dissolved in CH_2Cl_2 and precipitated by petroleum ether to give the pure product **30** without further purification. Yield 73%; ^{1}H NMR (400 MHz, CD_3OD): $\delta=8.27$ (s, 1H), 7.73 (m, 2H), 7.43 (m, 1H), 7.26 (t, $J=8$ Hz, 1H), 7.1 (t, $J=8$ Hz, 2H), 6.92 (q, $J=8$ Hz, 2H), 6.17 (s, 1H), 3.94 (t, $J=6$ Hz, 2H), 2.8 ppm (t, $J=6$ Hz, 2H); ^{13}C NMR (50 MHz, $CDCl_3$): $\delta=163.2$, 158.8, 145.5, 131.7, 130.4, 123.5, 123.5, 120.4, 117.3, 116.6, 116.1, 99.3, 61.4, 39.5, 30.8 ppm; MS (ESI) *m/z*: 368.4 $[M+H]^+$; Anal. calcd for $C_{19}H_{18}FN5O_2$: C 62.12, H 4.94, N 19.06, found: C 62.10, H 4.98, N 19.00.

Acknowledgements

This study was supported in part by the 6th FP Excellent-Hit Consortium (LSHP-CT-2006-037257) and by the Italian National Program of AIDS Research Grant 40H26 to G.M. This work was also supported by the European Union collaborative Projects "THINC" (grant no. HEALTH-2007-2.3.2-1), "CHAARM" (grant no. HEALTH-F3-2009-242135) and by the Italian Ministero dell'Istruzione, dell'Università e della Ricerca, Prin 2008 research project (grant no. 2008CE75SA 004). A.S. is supported by a fellowship from the "Franca Rame and Dario Fo" Nobel Foundation. Asinex is also acknowledged for partial financial support. F.B. thanks Ministero della Sanità, Fondazione IRCCS Policlinico San Matteo, and Ricerca Corrente (grants no. 80622) for financial support.

Keywords: antiviral agents · DDX3 · helicase · HIV-1 · host cofactors · inhibitors

[1] R. König, Y. Zhou, D. Elleder, T. L. Diamond, G. M. Bonamy, J. T. Irelan, C. Y. Chiang, B. P. Tu, P. D. De Jesus, C. E. Lilley, S. Seidel, A. M. Opaluch, J. S. Caldwell, M. D. Weitzman, K. L. Kuhen, S. Bandyopadhyay, T. Ideker, A. P. Orth, L. J. Miraglia, F. D. Bushman, J. A. Young, S. K. Chanda, *Cell* **2008**, *135*, 49–60.

[2] H. Zhou, M. Xu, Q. Huang, A. T. Gates, X. D. Zhang, J. C. Castle, E. Stec, M. Ferrer, B. Strulovici, D. J. Hazuda, A. S. Espeseth, *Cell Host Microbe* **2008**, *4*, 495 – 504.
[3] C. D. Pauza, D. N. Streblow, *Curr. Top. Microbiol. Immunol.* **1995**, *202*, 117 – 132.
[4] C. M. Hogan, S. M. Hammer, *Ann. Intern. Med.* **2001**, *134*, 978 – 996.
[5] A. D. Kwong, B. G. Rao, K.-T. Jeang, *Nat. Rev. Drug Discov.* **2005**, *4*, 845 – 853.
[6] A. Rosner, B. Rinkevich, *Curr. Med. Chem.* **2007**, *14*, 2517 – 2525.
[7] M. Schröder, *Biochem. Pharmacol.* **2010**, *79*, 297 – 306.
[8] M. Ishaq, J. Hu, X. Wu, Q. Fu, Y. Yang, Q. Liu, D. Guo, *Mol. Biotechnol.* **2008**, *39*, 231 – 238.
[9] Y. Ariumi, M. Kuroki, K. Abe, H. Dansako, M. Ikeda, T. Wakita, N. Kato, *J. Virol.* **2007**, *81*, 13922 – 13926.
[10] V. S. Yedavalli, C. Neuveut, Y. H. Chi, L. Kleiman, K. T. Jeang, *Cell* **2004**, *119*, 381 – 392.
[11] G. Maga, F. Falchi, A. Garbelli, A. Belfiore, M. Witvrouw, F. Manetti, M. Botta, *J. Med. Chem.* **2008**, *51*, 6635 – 6638.
[12] R. Franca, A. Belfiore, S. Spadari, G. Maga, *Proteins Struct. Funct. Bioinf.* **2007**, *67*, 1128 – 1137.
[13] M. Högbom, R. Collins, S. van den Berg, R. M. Jenvert, T. Karlberg, T. Kotenyova, A. Flores, G. B. Karlsson Hedestam, L. H. Schiavone, *J. Mol. Biol.* **2007**, *372*, 150 – 159.
[14] a) Asinex Ltd., 5 Gabrichevskogo St., Building 8, Moscow 125367 (Russia): http://www.asinex.com (accessed May 13, 2011); b) ChemBridge Corporation, 16981 Via Tazon, Suite G, San Diego, CA 92127 (USA): http://www.chembridge.com (accessed May 13, 2011).
[15] V. S. Yedavalli, N. Zhang, H. Cai, P. Zhang, M. F. Starost, R. S. Hosmane, K. T. Jeang, *J. Med. Chem.* **2008**, *51*, 5043 – 5051.
[16] L. T. Bogolyubskaya, V. A. Bogolyubskii, Z. P. Sytnik, *J. Org. Chem. USSR (Engl. Transl.)* **1966**, *2*, 1311 – 1313.
[17] M. Radi, L. Botta, G. Casaluce, M. Bernardini, M. Botta, *J. Comb. Chem.* **2010**, *12*, 200 – 205.
[18] G. A. Rogers, T. C. Bruice, *J. Am. Chem. Soc.* **1974**, *96*, 2463 – 2472.
[19] H. Jendralla, R. Henning, B. Seuring, J. Herchen, B. Kulitzscher, J. Wunner, *Synlett* **1993**, 155 – 157.
[20] a) M. Radi, S. Schenone, M. Botta, *Org. Biomol. Chem.* **2009**, *7*, 2841 – 2847; b) M. Radi, C. Falciani, L. Contemori, E. Petricci, G. Maga, A. Samuele, S. Zanoli, M. Terrazas, M. Castria, A. Togninelli, J. A. Esté, I. Clotet-Codina, M. Armand-Ugón, M. Botta, *ChemMedChem* **2008**, *3*, 573 – 593; c) M. Radi, L. Contemori, D. Castagnolo, R. Spinosa, J. A. Esté, M. Botta, *Org. Lett.* **2007**, *9*, 3157 – 3160; d) M. Radi, E. Petricci, G. Maga, F. Corelli, M. Botta, *J. Comb. Chem.* **2005**, *7*, 117 – 122.
[21] *SciFinder Scholar*, American Chemical Society: http://www.cas.org/products/sfacad/ (accessed May 13, 2011).
[22] GRID ver. 22, Molecular Discovery Ltd., Pinner, Middlesex, UK: http://www.moldiscovery.com/soft_grid.php (accessed May 13, 2011).
[23] G. Wolber, T. Langer, *J. Chem. Inf. Model.* **2005**, *45*, 160 – 169.
[24] A. Schüller, V. Hähnke, G. Schneider, *QSAR Comb. Sci.* **2007**, *26*, 407 – 410.
[25] C. S. Lee, A. P. Dias, M. Jedrychowski, A. H. Patel, J. L. Hsu, R. Reed, *Nucleic Acids Res.* **2008**, *36*, 4708 – 4718.
[26] G. A. Locatelli, S Spadari, G. Maga, *Biochemistry* **2002**, *41*, 10332 – 10342.
[27] E. Crespan, M. Radi, S. Zanoli, S. Schenone, M. Botta, G. Maga, *Bioorg. Med. Chem.* **2010**, *18*, 3999 – 4008.
[28] S. Paolucci, F. Baldanti, G. Maga, R. Cancio, M. Zazzi, M. Zavattoni, A. Chiesa, S. Spadari, G. Gerna, *Antimicrob. Agents Chemother.* **2004**, *48*, 4611 – 4617.
[29] D. Sun, M. Melegari, S. Sridhar, C. E. Rogler, L. Zhu, *Biotechniques* **2006**, *41*, 59 – 63.
[30] R. Gijsbers, K. Ronen, S. Vets, N. Malani, J. De Rijck, M. McNeely, F. D. Bushman, Z. Debyser, *Mol. Ther.* **2010**, *18*, 552 – 660.
[31] M. Geraerts, M. Michiels, V. Baekelandt, Z. Debyser, R. Gijsbers, *J. Gene Med.* **2005**, *7*, 1299 – 1310.
[32] Catalyst ver. 4.10 was formerly distributed by Accelrys Inc., and was recently re-engineered for improved usability in Discovery Studio: http://accelrys.com/products/discovery-studio/pharmacophores/ (accessed May 13, 2011).
[33] Cerius2 ver. 4.9 was formerly distributed by Accelrys Inc., and was recently re-engineered for improved usability in Discovery Studio: http://accelrys.com/products/discovery-studio/QSAR/ (accessed May 13, 2011).
[34] MacroModel ver. 8.5, Schrödinger LLC, New York, NY (USA), 2007: http://www.schrodinger.com/ (accessed May 13, 2011).
[35] W. L. Jorgensen, D. S. Maxwell, J. Tirado-Rives, *J. Am. Chem. Soc.* **1996**, *118*, 11225 – 11235.

Received: March 30, 2011
Revised: April 28, 2011
Published online on June 22, 2011

